Electronic Supplementary Information

Contrasting-functionality-decked robust MOF for moisture-tolerant and variable-temperature CO_2 adsorption with in-built urea group mediated mild condition cycloaddition

Manpreet Singh,[ab] Partha Pratim Mondal,[a] Sonal Rajput,[a] and Subhadip Neogi[ab*]

[a]Inorganic Materials & Catalysis Division, CSIR-Central Salt and Marine Chemicals Research Institute (CSIR-CSMCRI), Bhavnagar, Gujarat-364002, India
[b]Academy of Scientific and Innovative Research (AcSIR), Ghaziabad- 201002, India
*E-mail (SN): sneogi@csmcri.res.in , subhadip79@gmail.com

Table of content **Page S-**

Materials and physical measurements

All the solvents and reagents were purchased from commercial sources (except H_3TCA and ***L***) and used without further purification. H_3TCA and linker ***L*** were synthesised as per experimental section. Powder X-ray diffraction (PXRD) data were collected using a PANalytical Empyrean (PIXcel 3D detector) system equipped with Cu K_α (λ=1.54 Å) radiation. The Fourier Transform Infrared-spectra (IR) of the samples were recorded using the KBr pellet method on a Perkin–Elmer GX FTIR spectrometer in the region of 4000−400 cm^{-1}. Surface area and gas sorption measurement was carried out using Quantachrome Autosorb IQ instrument. Thermogravimetric analyses (TGA) (heating rate of 5 °C/min under N_2 atmosphere) were performed with a Mettler Toledo Star SW 8.10 system. ^1H and ^{13}C NMR spectra were recorded on a Bruker Avance-II 500 MHz NMR spectrometer. Scanning Electron Microscopic (SEM) and Transmission Electron Microscopic (TEM) images were obtained with a JEOL JSM 7100F and JEOL, JEM 2100 instrument, respectively. XPS analysis was carried out using a Thermo Scientific ESCALAB 250 Xi photoelectron spectrometer (XPS) using a monochromatic Al Kα X-ray as an excitation source. Inductively coupled plasma-optical emission spectrometry (ICP-OES) analysis was measured by Perkin Elmer, Optima 2000 Microanalyses of the compounds were conducted using elementarvario MICRO CUBE analyser.

Single crystal X-ray crystallography

Single crystals with suitable dimensions were chosen under an optical microscope and mounted on a glass fibre for data collection. The crystal data for as synthesized block shaped crystal of the framework were collected on a Bruker D8 Quest diffractometer, with CMOS detector in shutter less mode. The crystals were cooled to low temperature using an Oxford Cryostream liquid nitrogen cryostat. The instrument was equipped with a graphite monochromatized MoKα X-ray source (λ = 0.71073 Å), with Triumph™ X-ray source optics. Data collection and initial indexing and cell refinement were handled using APEX II software.[1] Frame integration, including Lorentz-polarization corrections, and final cell parameter calculations were carried out using SAINT+ software.[2] The data were corrected for absorption using the SADABS program.[3] Decay of reflection intensity was monitored by analysis of redundant frames. The structure was solved using Direct methods and difference Fourier techniques. All non-hydrogen atoms were refined anisotropically. All H atoms were placed in calculated positions using idealized geometries (riding model) and assigned fixed isotropic displacement parameters. The SHELXL-2014 package within the OLEX2 crystallographic software[4-7] was applied for structure refinement with several full-matrix least-squares/difference Fourier cycles. The disordered guest solvent molecules in the crystal lattice were treated with solvent mask option in OLEX2 software.[4] The potential solvent accessible void space was calculated using the PLATON[8] software. The crystal and refinement data framework is listed in Table S1. Topological analysis was performed by using TOPOSPro software.[9]

Experimental Section

Synthesis of ligands

4,4′,4″-tricarboxytriphenylamine (H_3TCA)

Ligand was synthesized and characterised by following similar protocol, reported from our group.[10]

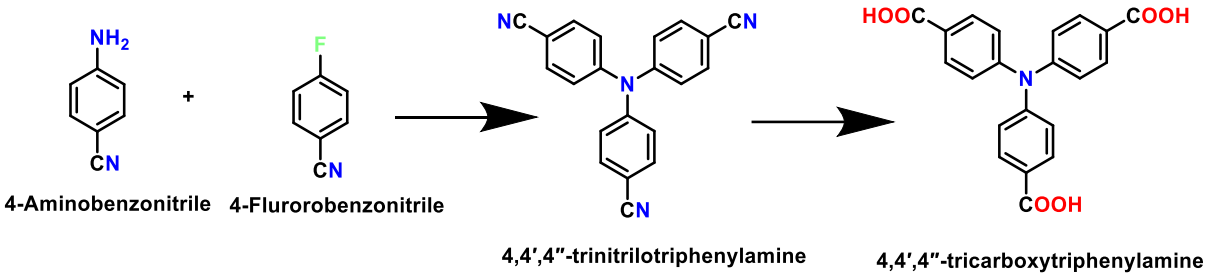

Scheme S1. Synthesis of C_3-symmetric ligand H_3TCA.

1,3-di(pyridin-4-yl)urea (*L*)

Ligand was synthesized and characterised by following similar protocol, reported from our group.[11]

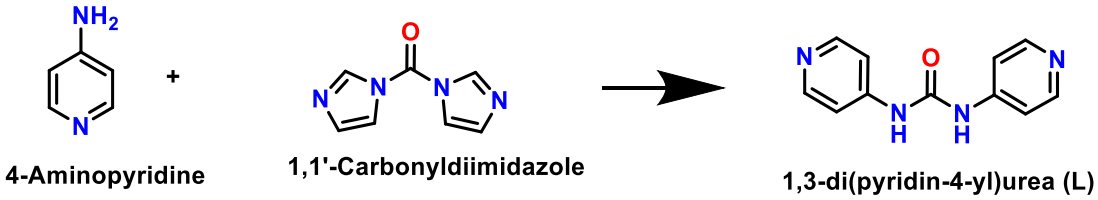

Scheme S2. Synthesis of Linker **L**.

Synthesis of the MOF

A mixture of $Cd(NO_3)_2 \cdot 4H_2O$ (30 mg, 0.1 mmol), Linker (***L***) (21.4 mg, 0.1mmol) and H_3TCA (19 mg, 0.05 mmol) was dissolved in the mixed solvent system (N,N-Dimethylacetamide: Water = 4 mL : 2 mL) in a 15 mL glass vial. The mixture was homogenised under ultrasonic treatment for 15 min. Followed by, heating it at 85 °C for 4 days, and then slowly cooled down to room temperature. The shiny, colourless, and rectangular block shaped X-ray quality crystals were obtained; which were then filtered, thoroughly washed with fresh DMA and air dried (yield: 75 %).

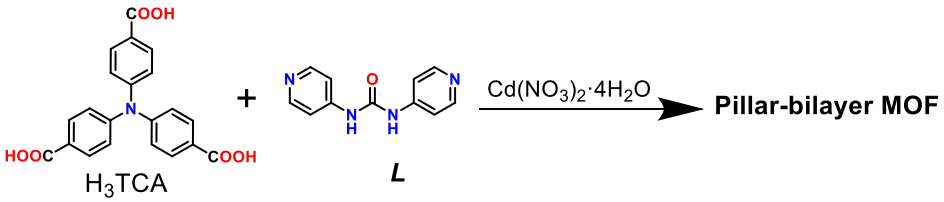

Scheme S3. Schematic illustration of MOF synthesis.

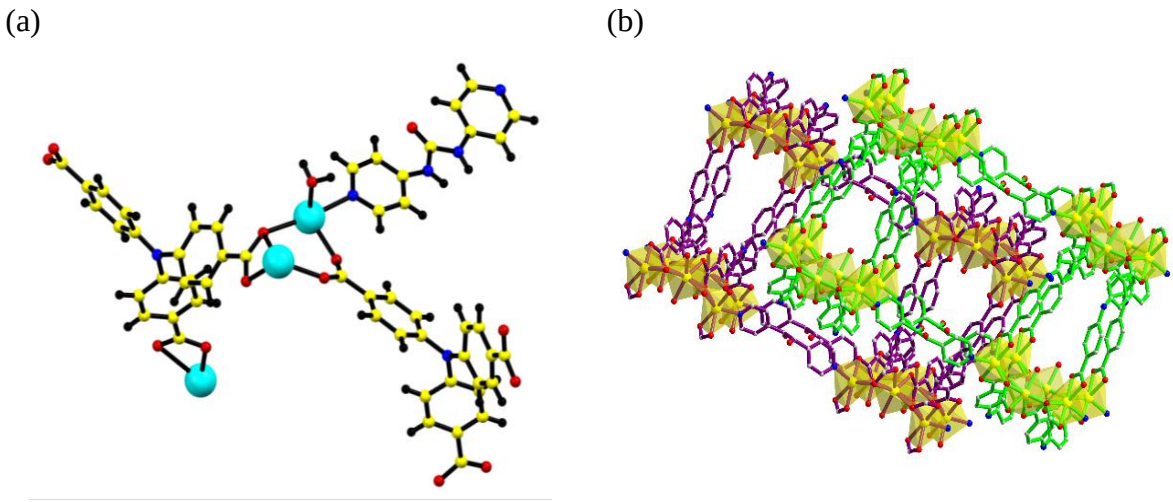

Fig. S1. (a)Asymmetric unit of the MOF and (b) representative figure of isostructural MOF [10] without urea functionality.

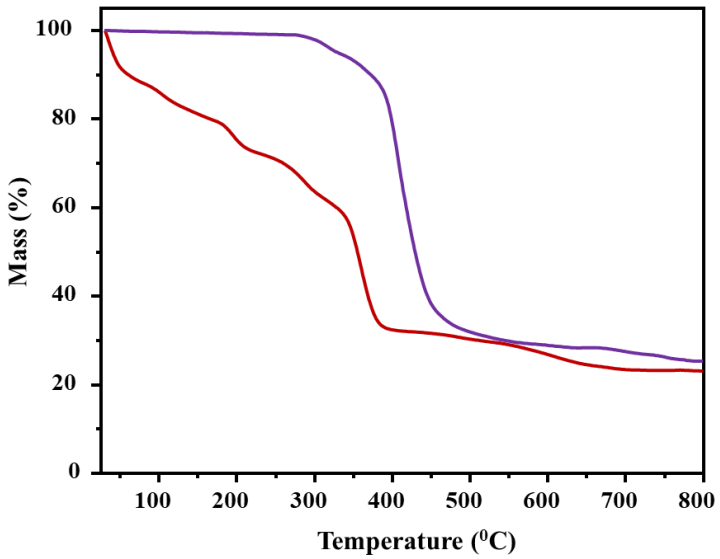

Fig. S2. Thermogravimetric curve of as-synthesized (red) and activated (purple) MOF.

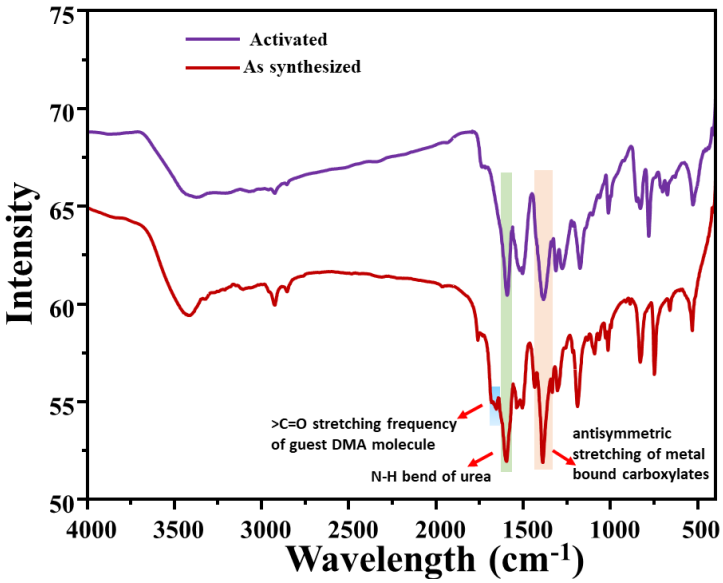

Fig. S3. FTIR spectra of as-synthesized (red) and activated (purple) MOF.

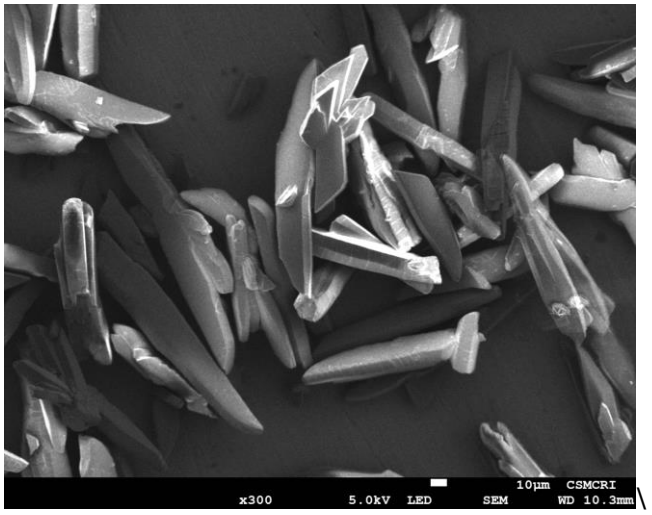

Fig. S4. SEM image of the activated framework.

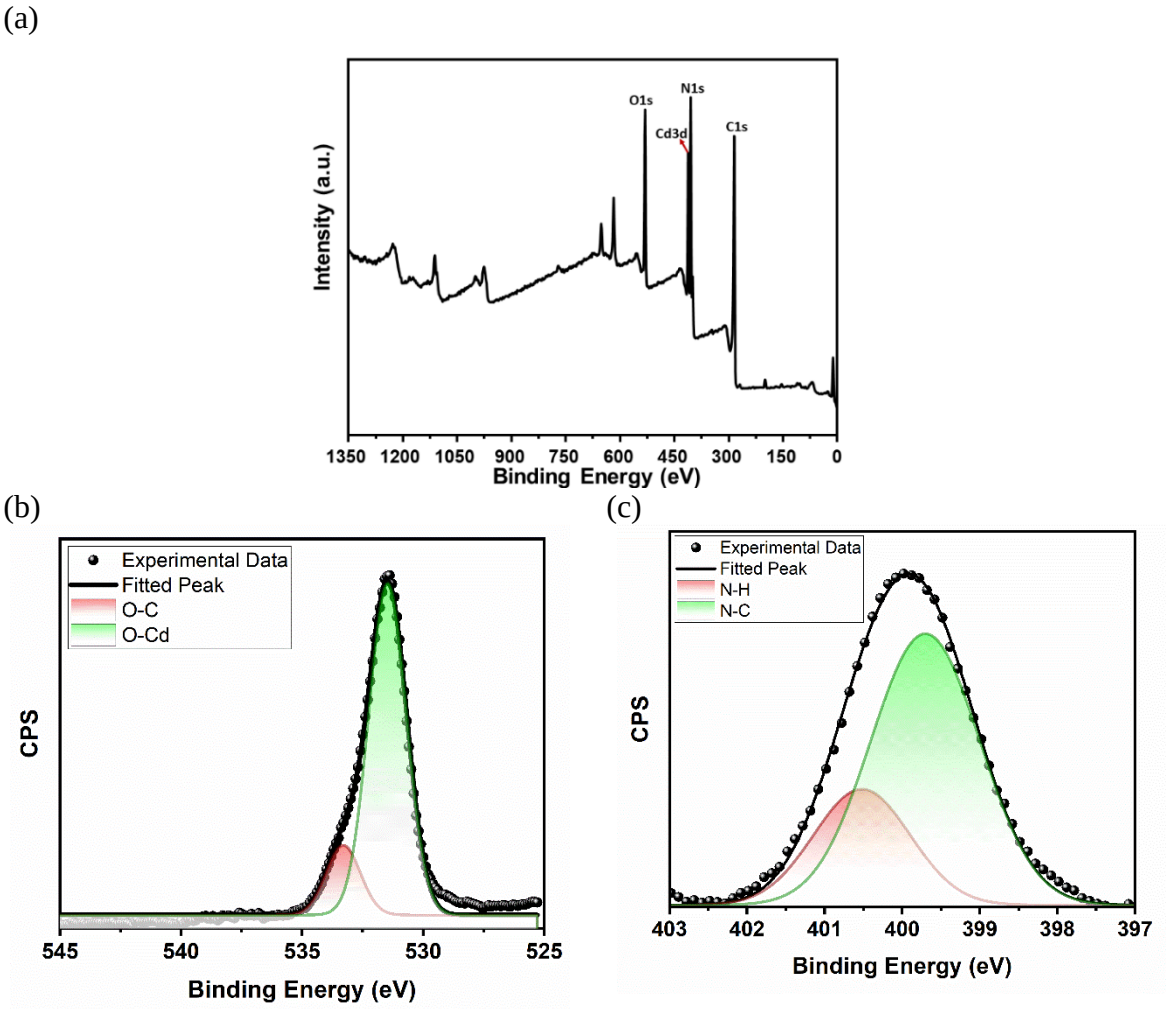

Fig. S5. (a) XPS survey spectra of the MOF along with deconvoluted high resolution spectra of (b) O 1s, and (c) N 1s.

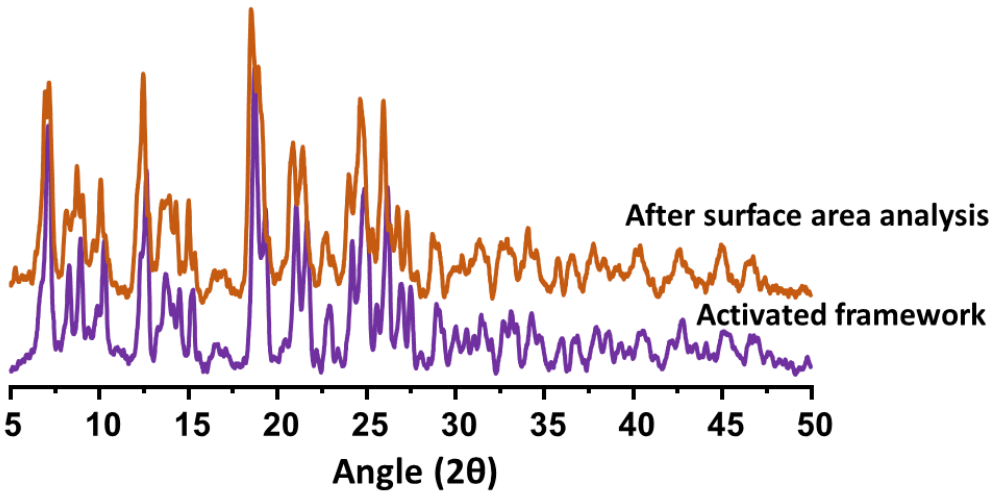

Fig. S6. Intact PXRD pattern of the MOF after surface area measurement.

Calculation of Heat of adsorption (Q_{st})

Clausius Clapeyron equation was employed for calculation of heat of adsorption (ΔH_{ads}). In order to use this equation, two data points are required for both temperature and pressure are required respectively. Data at 273 K & 298 K in the pressure range from 0-1 bar with constant uptake was fit in the equation.

$$ln\frac{P_2}{P_1} = \frac{\Delta H_{ads}}{R}\left(\frac{T_2 - T_1}{T_2 T_1}\right) \quad \text{.....(Equation S1)}$$

Where,

ΔH_{ads} = Isosteric heat of adsorption,

R = universal gas constant,

P = pressure,

T = temperature.

The ΔH_{ads} is obtained as a function of uptake by using above equation and adsorption isotherms measured as shown in main text and this was carried out with a linear interpolation method, as shown below.

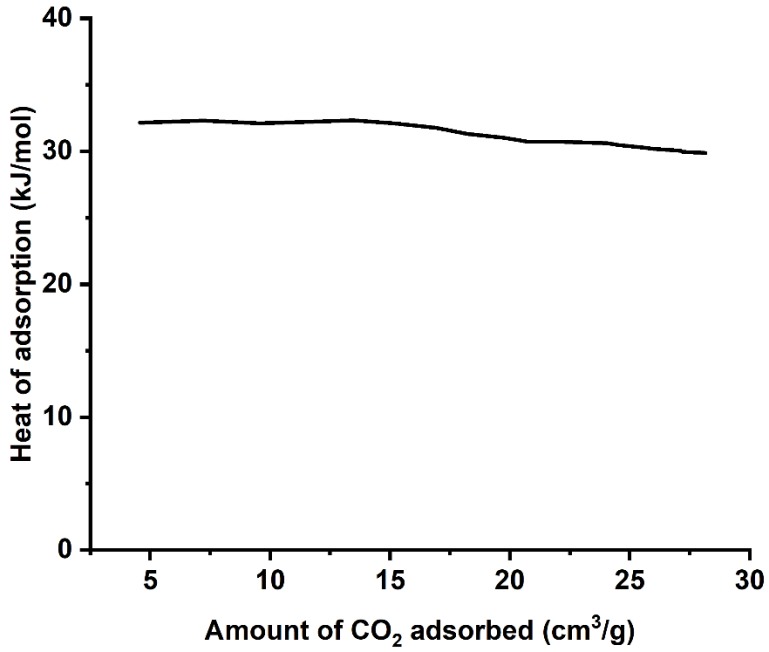

Fig. S7. Heat of adsorption curve of CO_2 adsorption for activated framework.

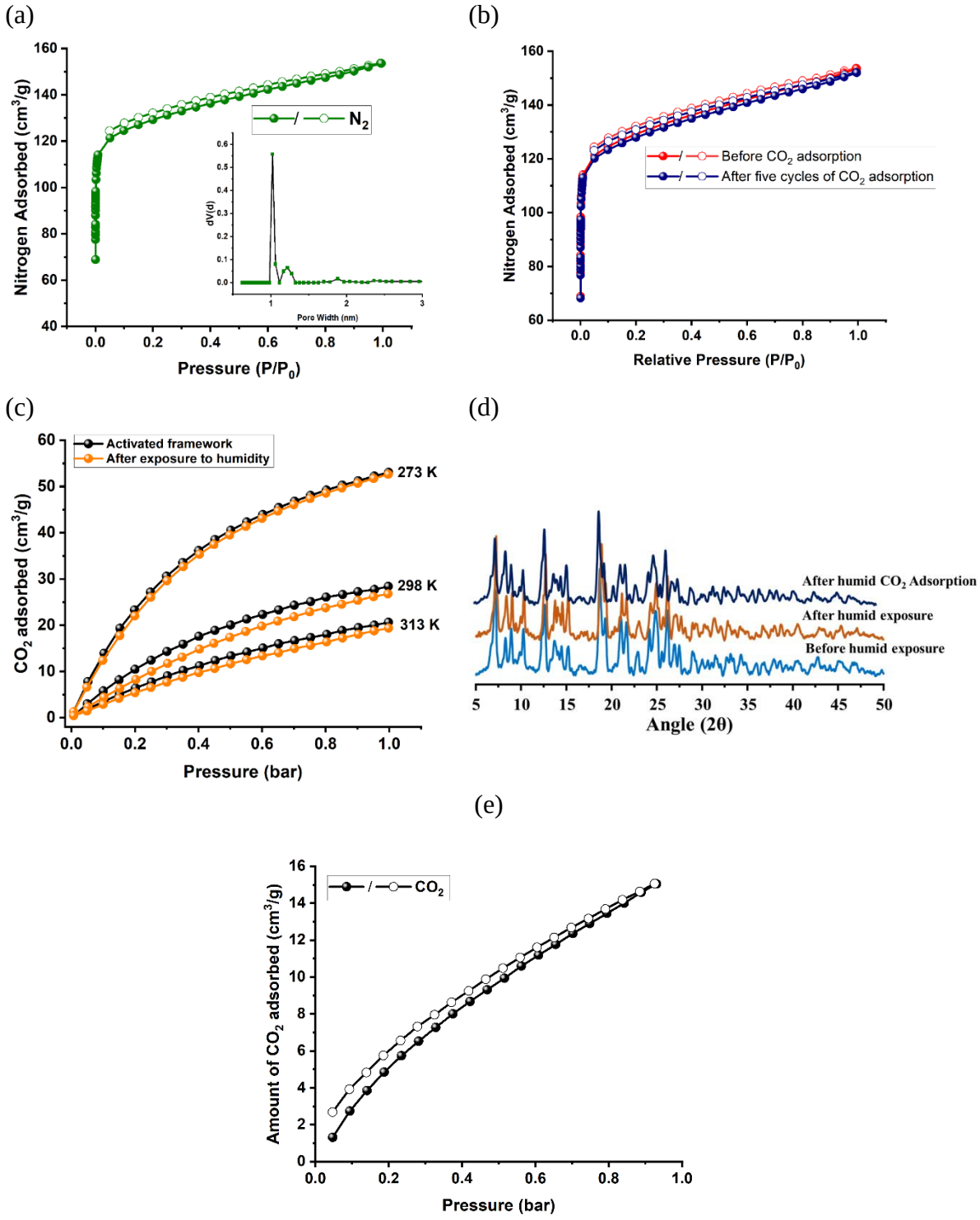

Fig. S8. (a) N_2 adsorption isotherm at 77 K for the activated framework, (b) N_2 adsorption isotherms before and after CO_2 adsorption, (c) Amount of CO_2 adsorbed before (black) and after (orange) exposure to humidity at different temperature, and (d) PXRD pattern before (humid exposure) after (humid exposure) and after CO_2 adsorption (e) CO_2 adsorption-desorption isotherm at 273 K for the un-functionalized framework.

Calculations of Adsorption Selectivity by IAST method

In order to predict mixed-gas adsorption equilibria from single –component isotherm Ideal Adsorption Solution Theory (IAST) was used. Langmuir equation (give below) was successfully used for fitting our data.

$$q = \frac{q_m bp}{1+bp} \text{ …..(Equation S2)}$$

q - adsorbed amount per mass of adsorbent
q_m - saturation capacity
b - affinity coefficient of adsorption sites
p - pressure of the bulk gas at equilibrium with the adsorbed phase
The fitted parameters were then used to predict single-component adsorption with IAST.
The inputs to the IAST calculations are pure-component adsorption isotherms at the temperature of interest, and the output is the adsorption selectivity is defined by the following equation,

$$S_{ads} = \frac{q_{CO_2}/q_{Other}}{p_{CO_2}/p_{other}} \text{…… (Equation S3)}$$

Where, q_{CO_2} and q_{Other} are the absolute component loadings of the adsorbed phase in the mixture and p_{CO_2} and p_{other} are the corresponding relative pressure.

Table S1. Langmuir fitting parameters for the activated framework.

Gas (Analysis Temp)	**q_m**	**b**
CO_2 (273 K)	77.4	2.17
CO_2 (298 K)	49.7	1.36
CO_2 (313 K)	46.13	0.8
CH_4 (273 K)	65.3	0.29
CH_4 (298 K)	10.9	0.76
CH_4 (313 K)	6.79	0.76
N_2 (273 K)	3.27	0.19
N_2 (298 K)	1.14	0.19
N_2 (313 K)	0.53	0.19

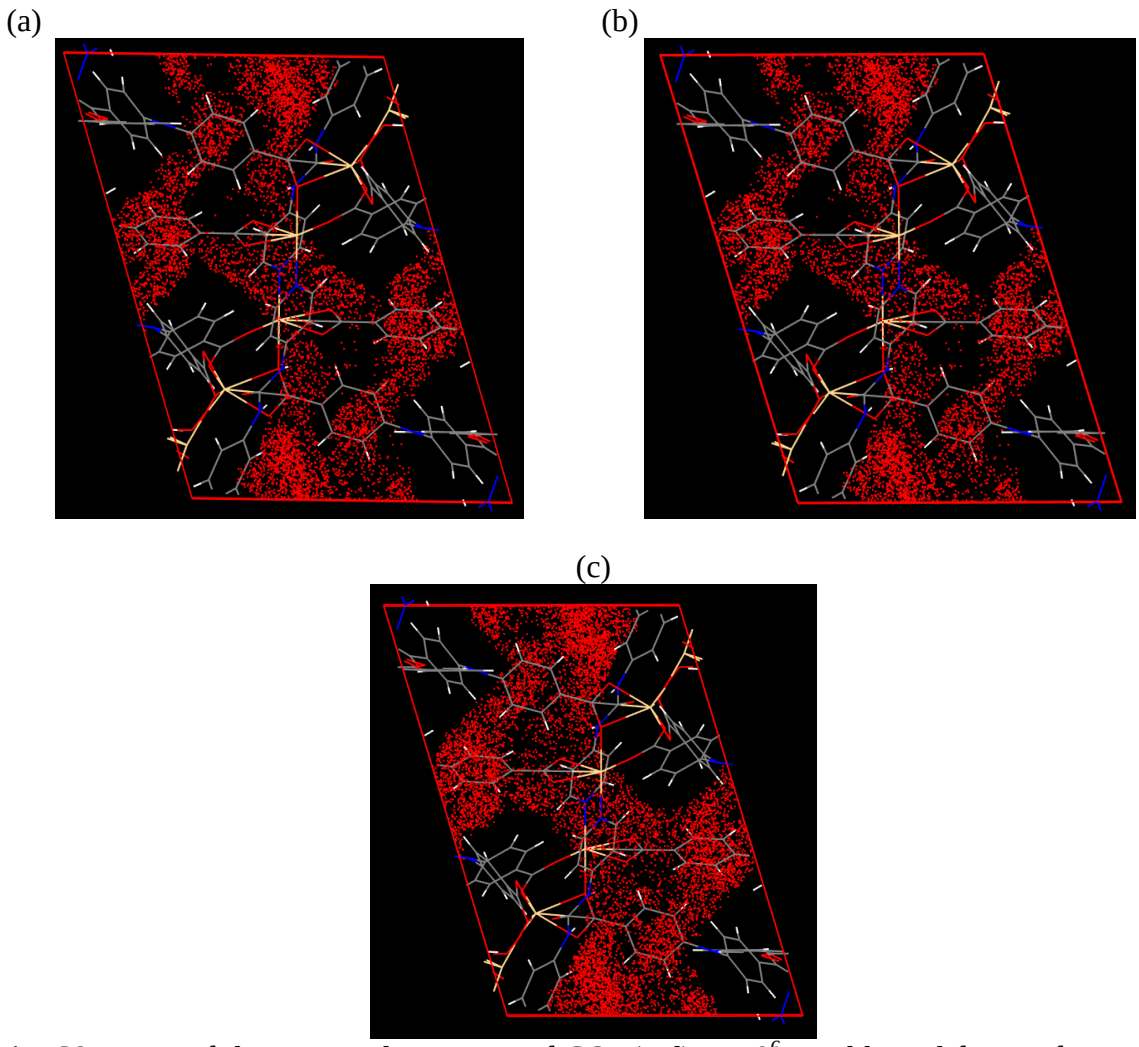

Fig. S9. Maps of the occupied positions of CO_2 (red) in 10^6 equilibrated frames for a given pressure of 1 bar at (a) 273 K (b) 298 K & (c) 313 K.

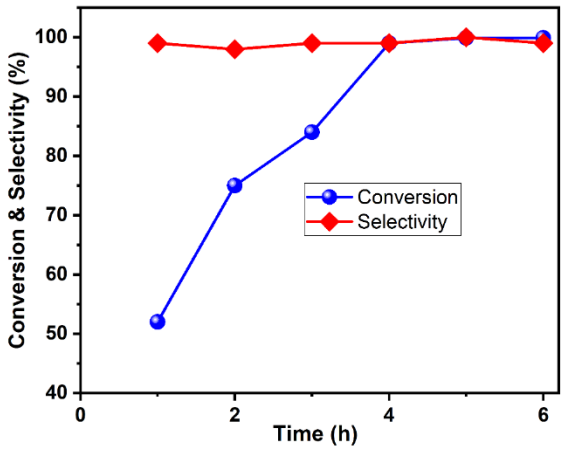

Fig. S10. Optimization of reaction time on the conversion and selectivity of styrene oxide. (Reaction conditions: epoxide, 26.46 mmol; MOF, 0.25 mol %; $Bu_4N^+Br^-$, 0.2 mol %; CO_2 pressure, 0.5 MPa; temp, 50 °C; Selectivity > 99%)

Yield calculation for CO_2 cycloaddition reaction catalyzed by activated MOF:

For styrene carbonate the formula are

Conversion (%) = $[1-\{5I_{Ha}/I_{H(b-f)}\}]\times 100$ %

Yield (%) = $\{5I_{Ha'}/I_{H(b-f)}\}\times 100$ %

From Fig. S7, for styrene carbonate, I_{Ha}= 0.00, $I_{Ha'}$ = 1.00 and $I_{H(b-f)}$ = 5

Therefore, conversion (%) = $\{1-(5\times 0.00/4.99)\}\times 100$ % = 100 %

Yield (%) = $(5\times 1/5)\times 100$ % = 100 %

Conversion and yield were calculated by integrating the characteristic proton signals of epoxide and cyclic carbonate molecules in their ^{1}H NMR spectra and applying the following formula.

Conversion (%) = $\{I_{Ha'}/ (I_{Ha}+I_{Ha'})\} \times 100$ %

Yield (%) = $\{I_{Ha}/(I_{Ha}+I_{Ha'})\} \times 100$ %

From Fig. S10, for propylene carbonate, I_{Ha}= 0.00, $I_{Ha'}$ = 1.00

Therefore, conversion of propylene oxide = yield of propylene carbonate = $\{1/(1+0.00)\} \times 100$ % = >99 %

(a)

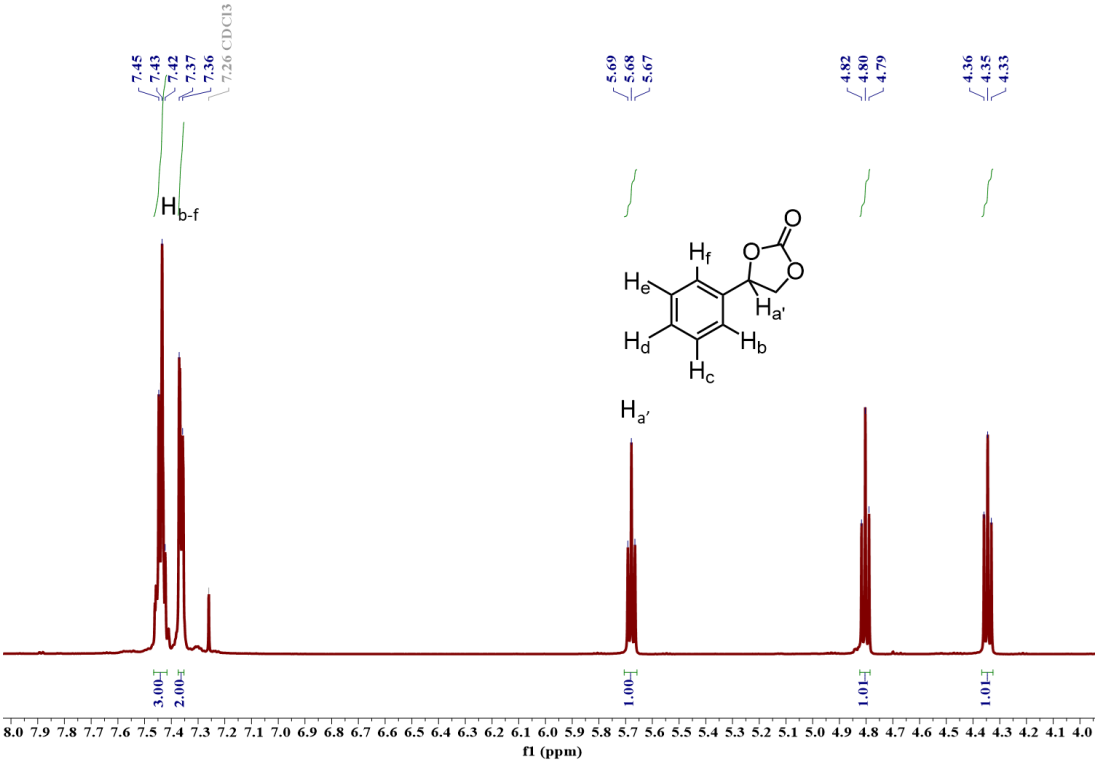

(b)

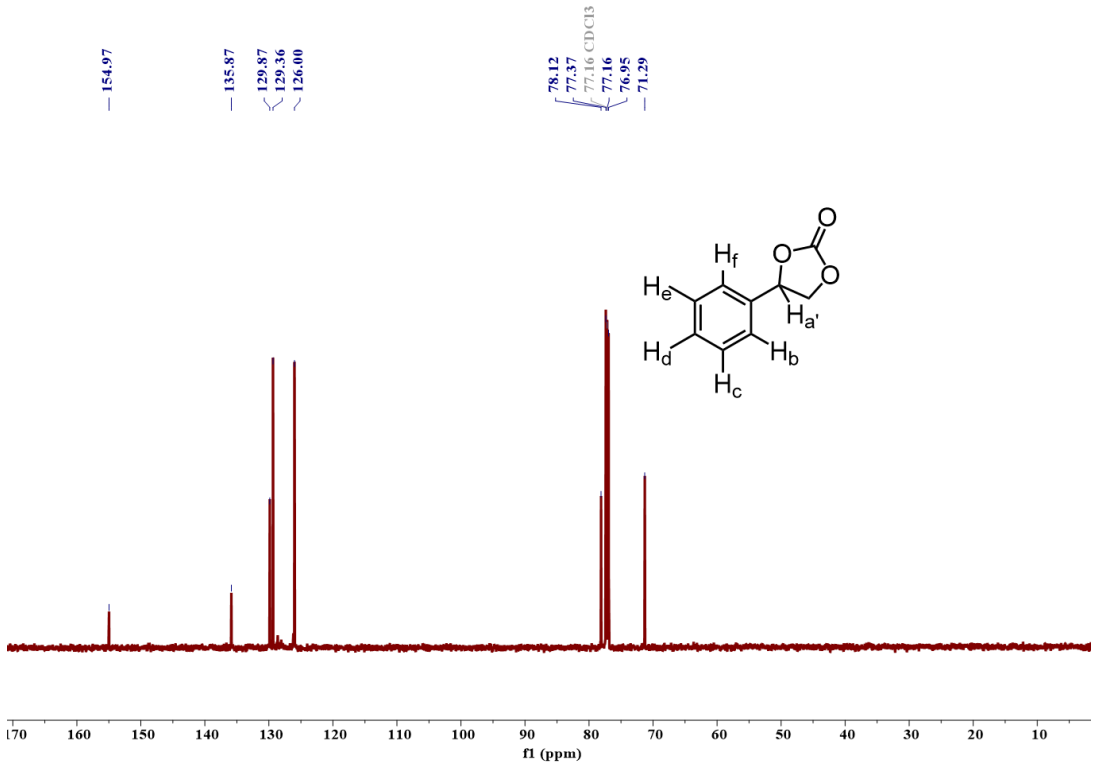

Fig. S11. NMR spectra of styrene carbonate (4-Phenyl-1,3-dioxolan-2-one) (a) ^{1}H & (b) ^{13}C in $CDCl_3$.

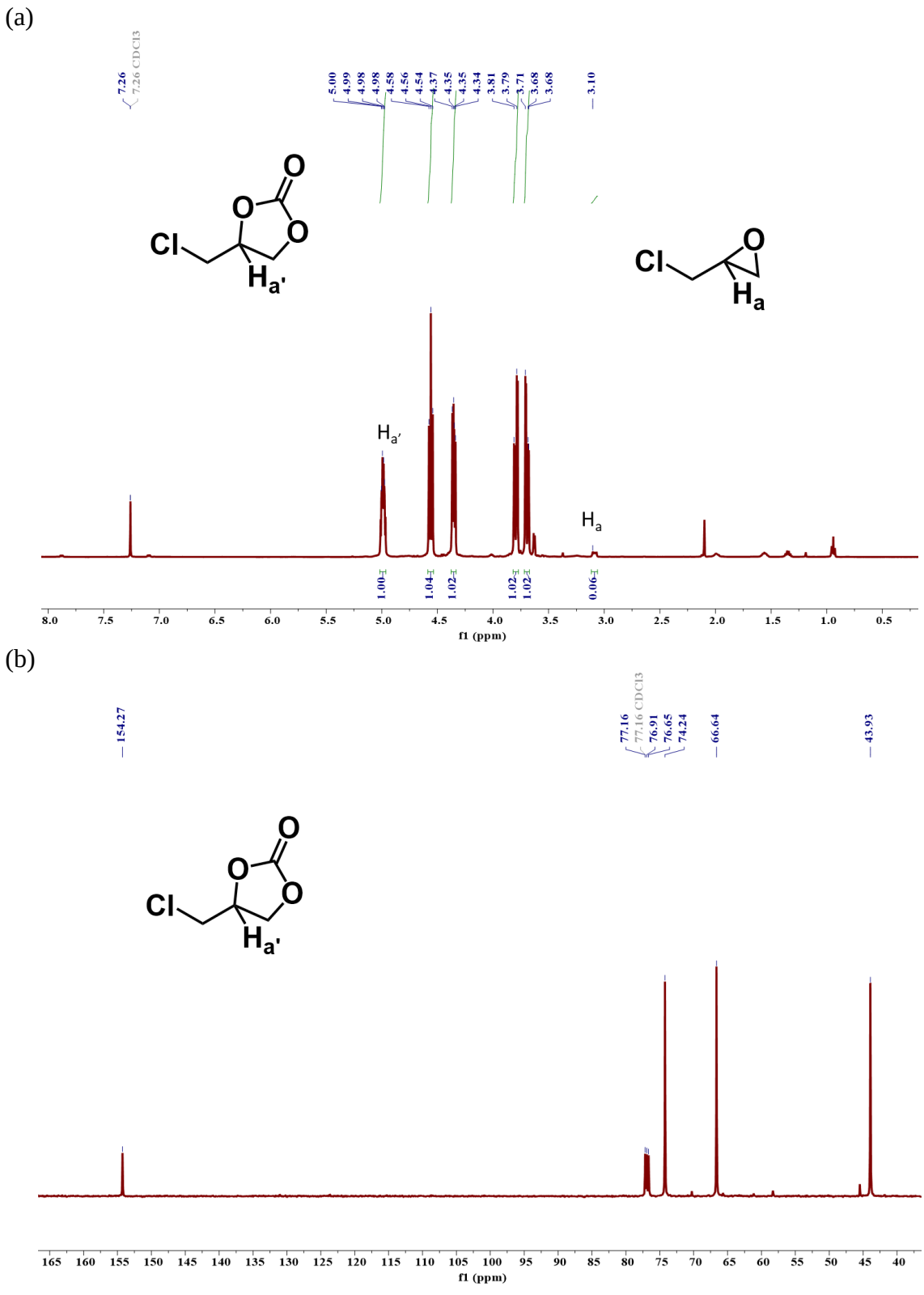

Fig. S12. NMR spectra of epichlorohydrin carbonate (4-(chloromethyl)-1,3-dioxolan2-one) (a) ^{1}H & (b) ^{13}C in $CDCl_3$.

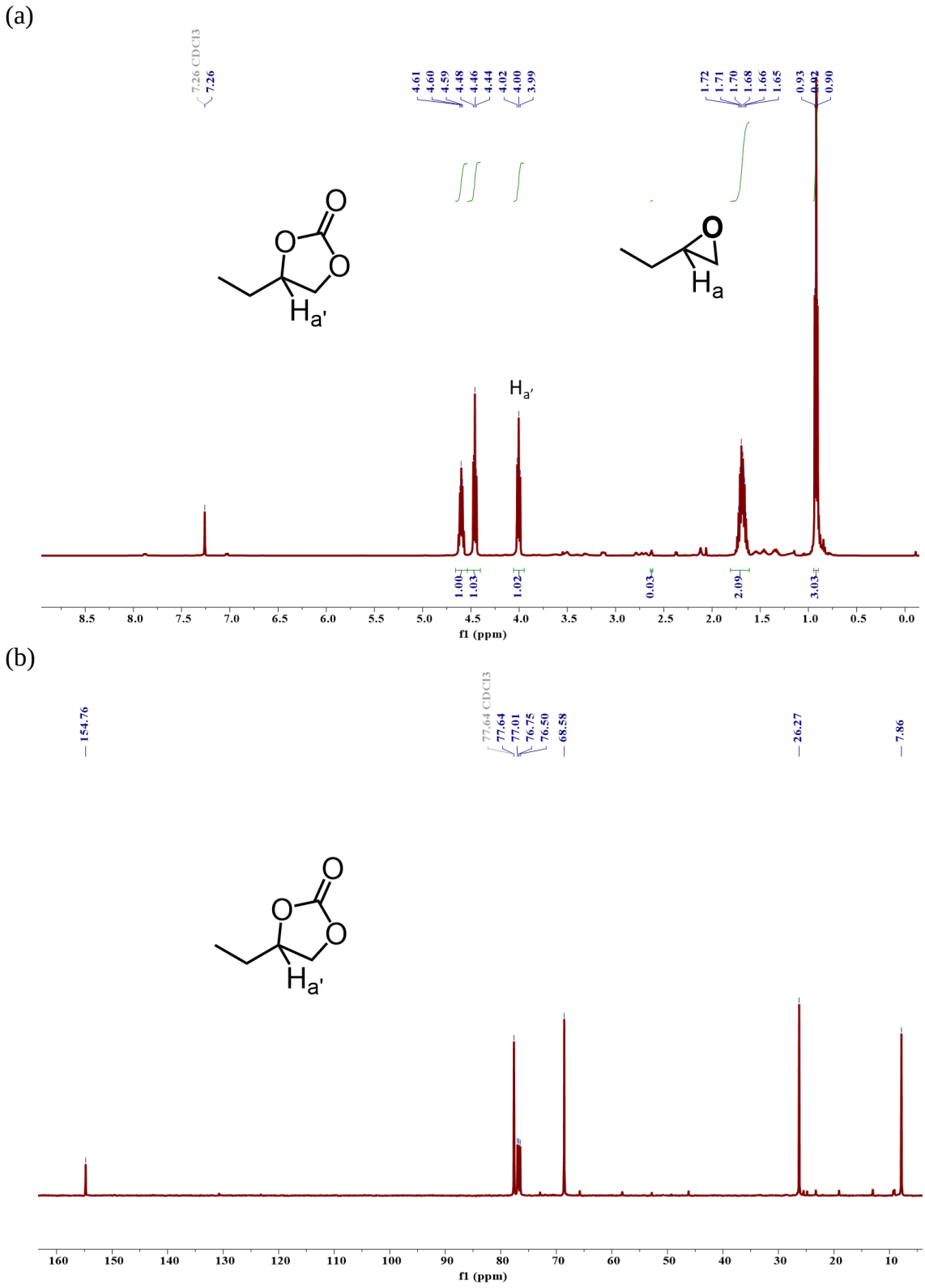

Fig. S13. NMR spectra of butylene carbonate (4-Ethyl-1,3-dioxolan-2-one) (a) ^{1}H & (b) ^{13}C in $CDCl_3$.

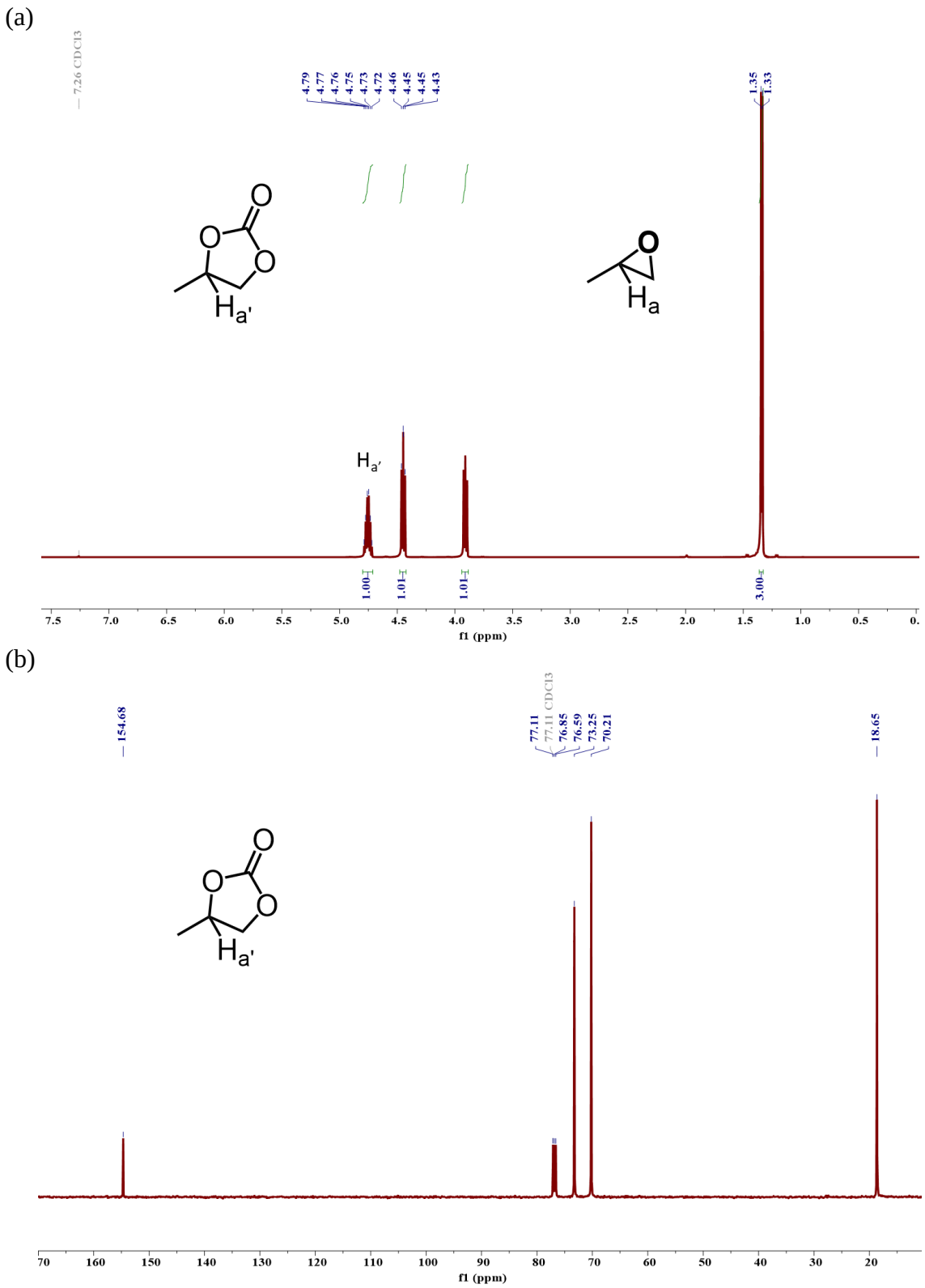

Fig. S14. NMR spectra of propylene carbonate (4-Methyl-1,3-dioxolan-2-one) (a) ^{1}H & (b) ^{13}C in $CDCl_3$.

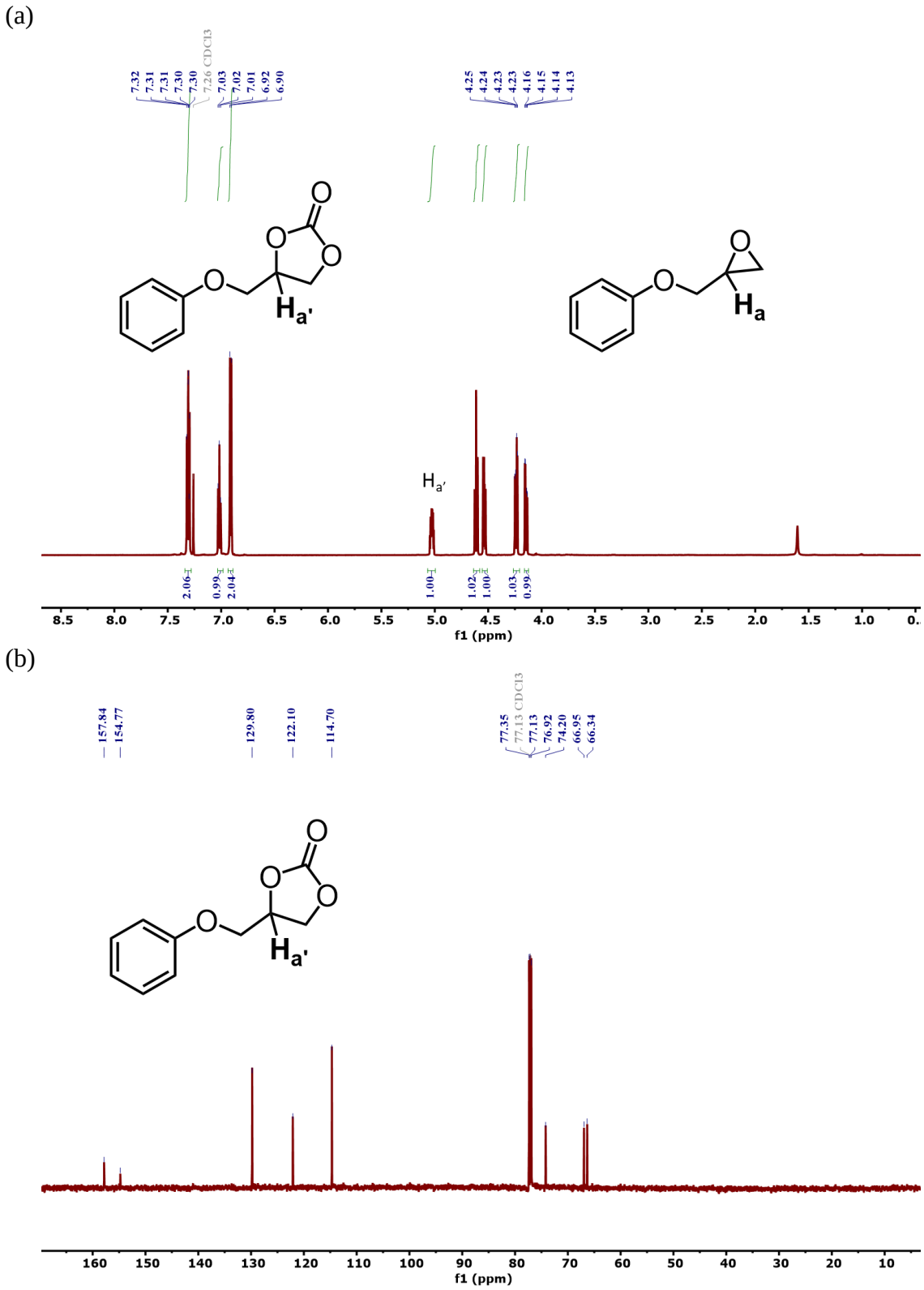

Fig. S15. NMR spectra of phenyl glycidyl carbonate (4-(phenoxymethyl)-1,3- dioxolan-2-one) (a) ^{1}H & (b) ^{13}C in $CDCl_3$.

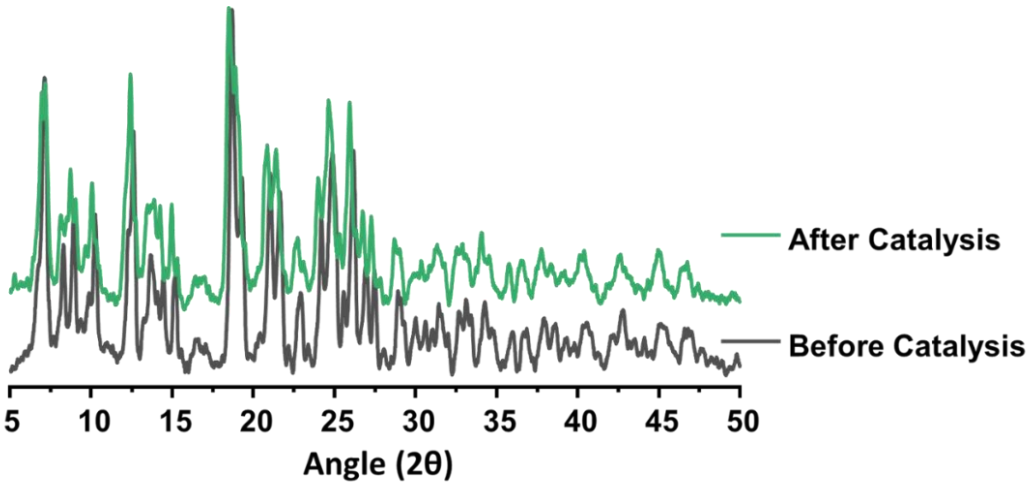

Fig. S16. PXRD pattern of the MOF before (black) and after (green) catalysis.

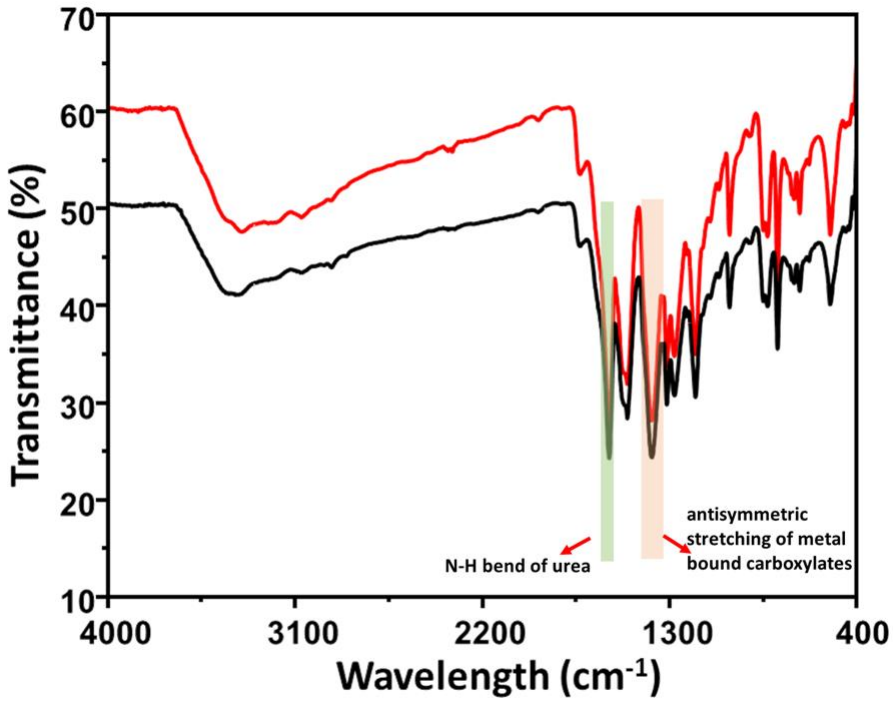

Fig. S17. FTIR spectra of the MOF before (black) and after (red) catalysis.

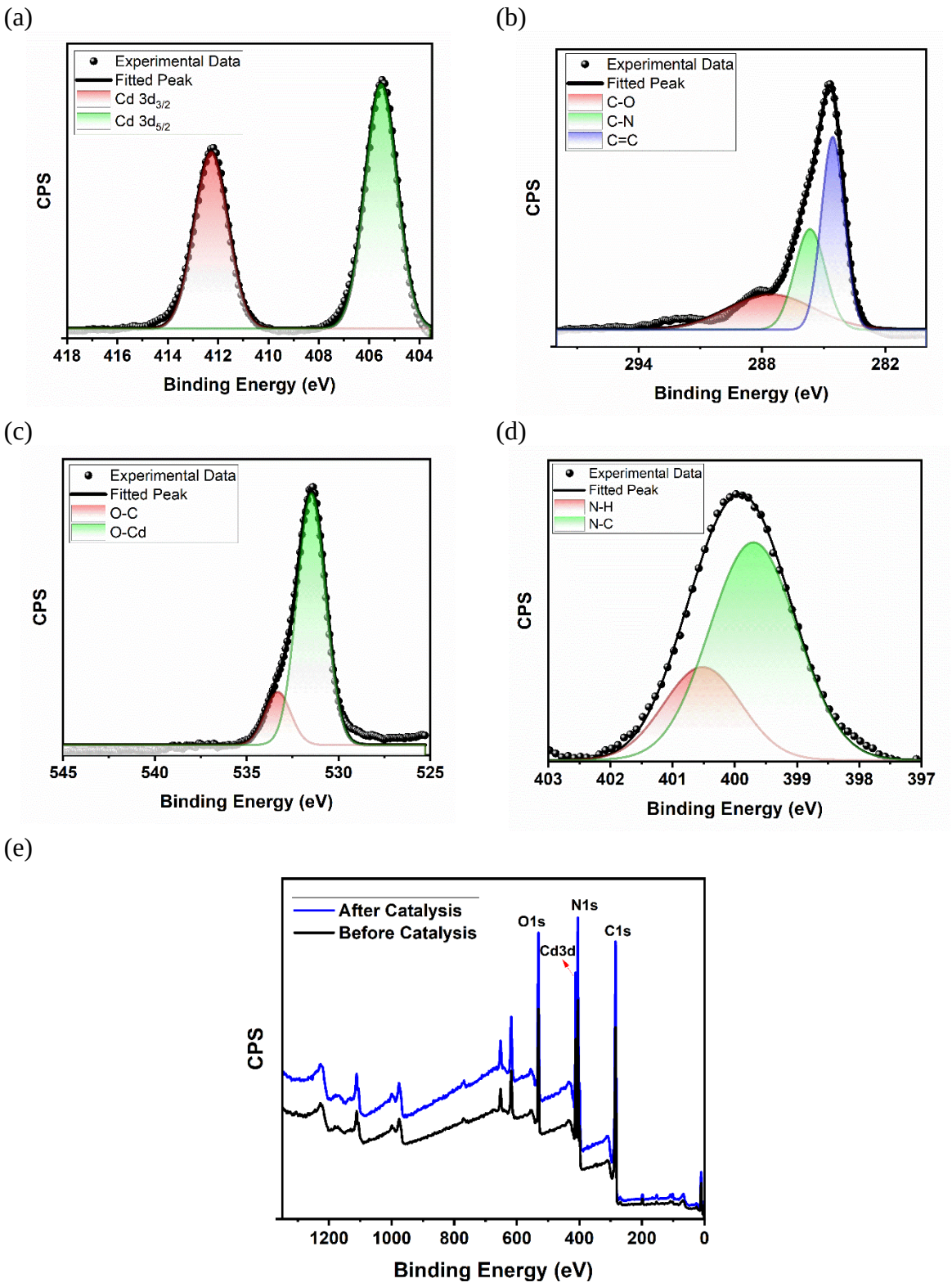

Fig. S18. XPS spectra of MOF after catalysis: deconvoluted spectra of (a) Cd 3d, (b) C 1s, (c) O 1s, (d) N 1s and (e) Intact XPS survey spectra of the framework post catalysis.

(a)

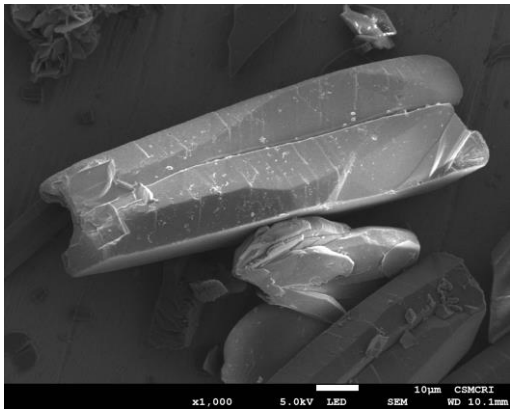

(b)

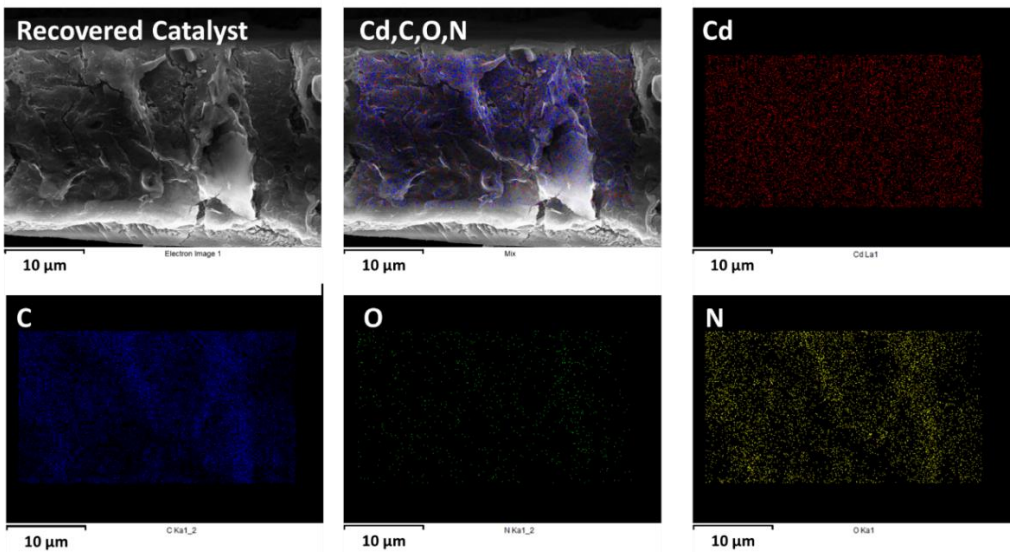

Fig. S19. (a) SEM images of the catalyst post catalysis and (b) Elemental mapping showing uniform distribution of elements (mix, Cd, C, O, N) in the selected area of the MOF crystal after catalysis.

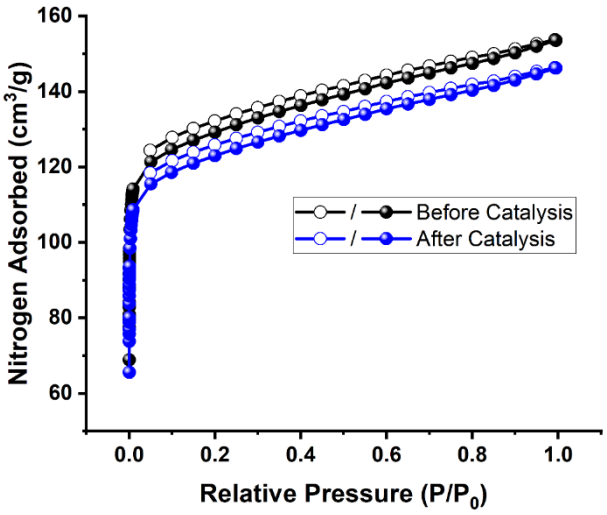

Fig. S20. N_2 adsorption isotherm of the MOF before and after five cycles of catalysis.

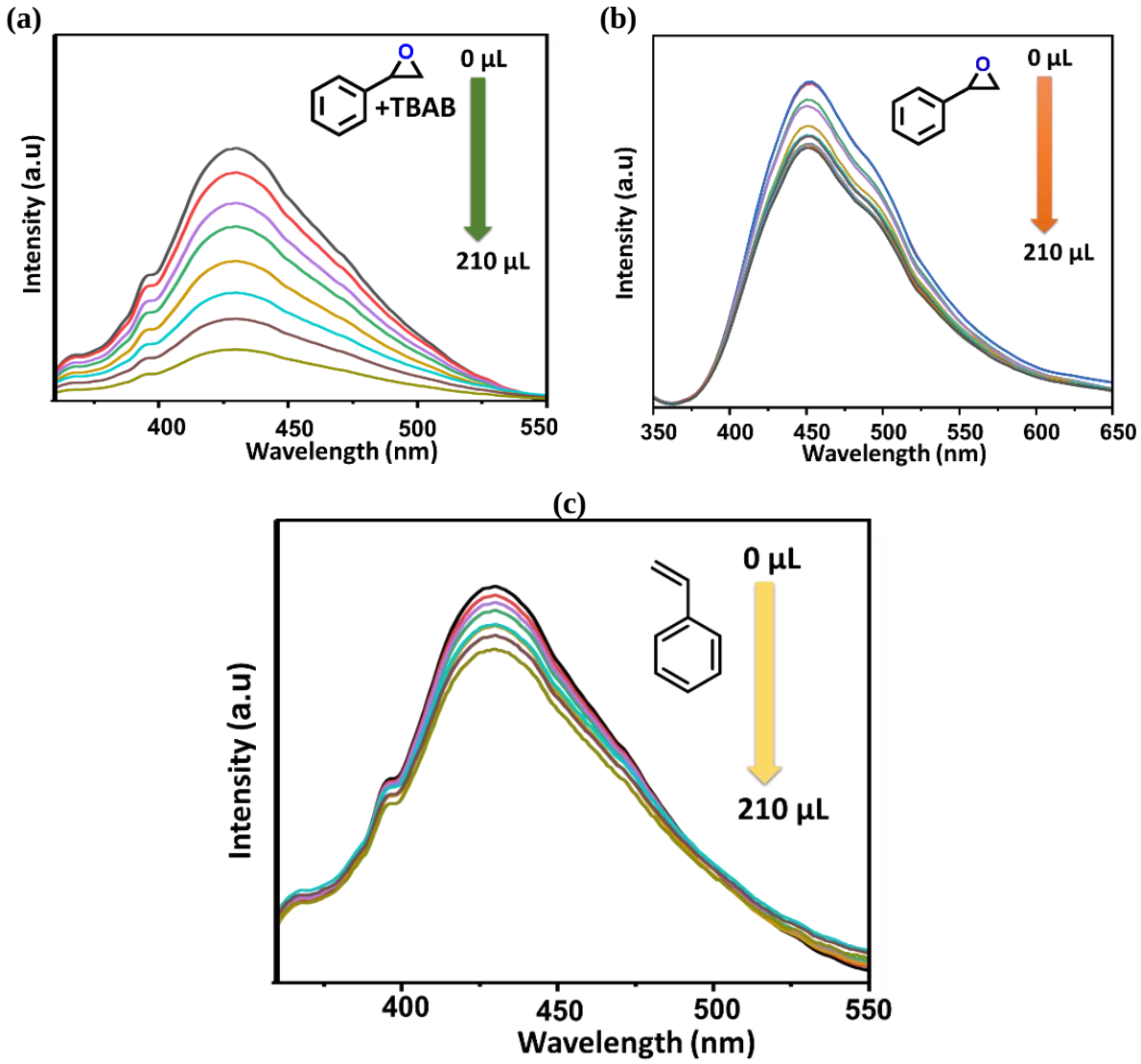

Fig. S21. Emission spectrum of (a) activated framework with styrene epoxide in presence of TBAB (b) isoskeletal framework in presence of styrene epoxide (c) activated framework with styrene.

Table S2. Crystal data and refinement parameters for the MOF.

Identification code	MOF
Empirical formula	C_{53} H_{38} Cd_3 N_6 O_{15}
Formula weight	1336.16
Temperature/K	180.15
Crystal system	triclinic
Space group	*P*-1
a/Å	14.7456(3)
b/Å	14.8727(3)
c/Å	19.8711(5)
α/°	95.8630(10)
β/°	103.1660(10)
γ/°	112.2630(10)
Volume/Å^3	3840.17(15)
Z	2
ρ_{calc}g/cm^3	1.1555
μ/mm^{-1}	0.874
F(000)	1319.8
Crystal size/mm^3	0.232 × 0.087 × 0.034
Radiation	Mo Kα (λ = 0.71073)
2Θ range for data collection/°	4.72 to 52.82
Index ranges	-18 ≤ h ≤ 18, -18 ≤ k ≤ 18, -24 ≤ l ≤ 24
Reflections collected	144882
Independent reflections	15381 [R_{int} = 0.0700, R_{sigma} = 0.0389]
Data/restraints/parameters	15381/0/697
Goodness-of-fit on F^2	1.028
Final R indexes [I>=2σ (I)]	R_1 = 0.0470, wR_2 = 0.1355
Final R indexes [all data]	R_1 = 0.0619, wR_2 = 0.1437
Largest diff. peak/hole / e Å^{-3}	0.89/-1.13

Explanation for the alerts

Alert level B:

PLAT420_ALERT_2_B D-H Bond Without Acceptor O1 --H1A . Please Check
PLAT420_ALERT_2_B D-H Bond Without Acceptor O1 --H1B . Please Check
PLAT420_ALERT_2_B D-H Bond Without Acceptor O01A --H01A . Please Check
PLAT420_ALERT_2_B D-H Bond Without Acceptor O01A --H01B . Please Check

Explanations: The atom pairs correspond to the O-H groups of metal-coordinated water molecules. These alerts were generated due to a common error of an -OH with hydrogen atom on a calculated position with O-H pointing in the wrong direction.

PLAT910_ALERT_3_B Missing # of FCF Reflection(s) Below Theta(Min). 12 Note

Explanations: This alert was generated due to omission of some reflections in the refinement process for technical reasons.[12]

PLAT934_ALERT_3_B Number of (Iobs-Icalc)/Sigma(W) > 10 Outliers .. 10 Check

Explanations: This alert is due to a consequence of weak data quality.[12, 13]

Determination of formula & solvent composition of the MOF from PLATON and TGA

From the TGA plot of as-synthesized MOF, the observed mass loss is 21.27 %
From PLATON Squeeze program, void electron count / unit cell turns out to be 206.
Now, formula of the asymmetric unit (SCXRD) excluding all lattice guest molecules is $[Cd_3(TCA)_2\boldsymbol{L}(H_2O)_2]$, with corresponding mass: 1334.13

Table S3. Number of electrons and molecular mass of guest molecules, associated with MOF for determination of solvent composition and molecular formula.

	Dimethyl acetamide (DMA)	Water
No. of electrons count	48	10
mass	82	18

Considering the above-mentioned number of electrons, the best possible combination of solvent molecules for this MOF could be $[Cd_3(TCA)_2\boldsymbol{L}(H_2O)_2]\cdot 2DMA\cdot 11H_2O$
The total number of electrons contributed by lattice solvent molecules will be [2×(48) + (10×11)] = 206, which is in agreement with the PLATON result, and validates this formula.
The aforementioned combination was further cross-checked from TGA analysis.
Total mass loss due to solvents is [2× (82) + (11×18)] = 362
Therefore, total mass of MOF including all the guests is (1334.13+362) = 1696.13
Therefore, mass loss due to solvents is [(362/1696.13) ×100] % = 21.34 %, which is also comparable to that of the TGA result.
From elemental analysis, calculated C: 42.88, H: 4.60, N: 6.56 and found C: 42.81, H: 4.64, N: 6.55

	No. of moles of C	No. of moles of H	No. of moles of N
Calculated	42.88/12.01 = 3.57	4.60/1.0079 = 4.56	6.56/14.0067 = 0.46
Experimental	42.81/12.01 = 3.56	4.64/1.0079 = 4.6	6.55/14.0067 = 0.46

Therefore, calculated mole ratio of C, H, N is 7.76:9.91:1, while found mole ratio is 7.73:10:1, which are in good agreement, thus validating the above formula.

Table S4. List of metal-organic frameworks and their corresponding surface area and CO_2 adsorption capacity at 237 K up to a pressure of 1 bar.

S.No.	Chemical formula	Common name	BET	Capacity	- *Qst*	Selectivity		Ref.
			(m^2/g)	(cm^3/g)	$kJmol^{-1}$	CO_2/N_2	CO_2/CH_4	
1.	$Er_2(PDA)_3$	-	-	11.71	30.1	-	-	14
2.	$[NH_2(CH_3)_2][Zn_3(BTA)(BTC)_2(H_2O)]$	-	697	102	-	11.2	3.1	15
	$[NH_2(CH_3)_2]_2[Cd_3(BTA)(BTC)_2(H2O)]_2$		508	84		12	3.1	
3.	$[Cd(bpydc)_2(DMF)_2{\cdot}2DMF]_n$ (JMS-3)	JMS-3a		30.89	34.4	-	-	16
	$[Zn(bpydc)(DMF){\cdot}DMF]_n$ (JMS-4)	JMS-4a		16.08	30.7	-	-	
4.	$[Sc_3(\mu_3\text{-}O)(L)_{1.5}(H_2O)_3Cl]_n$	NJU-Bai49	1189	137.5	33.4	-	-	17
5.	$[Co^{II}_4(\mu\text{-}OH_2)_4(MTB)_2{\cdot}(H_2O)_4]_n$ $\cdot 13n DMF \cdot 11n H_2O$	SNU-15	356	35.7	-	-	-	18
6.	$CuB(4\text{-}MIm)_4$	BIF-8-Cu	1287	34.1		-	-	19
	$LiB(4\text{-}MIm)_4$	BIF-9-Li	1523	35.6	-	-	-	
7.	$[Zn_2(btm)_2]{\cdot}4H_2O$	MAF-23	622***	74.2	47.4	82	-	20
8.	-	UiO-66(Zr)-$(SH)_2$	308	-		-	-	21
9.	$[Cu(bpy)_2(EDS)]_n$	TMOF-1	256	47.1	30.9	-	-	22
10.	$[Zn_2(L)(oba)_2]{\cdot}3DMA{\cdot}2CH_3OH{\cdot}3H_2O$	CSMCRI-16	599**	85.79	24.62	155.3	3.1	23
11.		NUM-3a	2111	113	24.1	82.8	11	24
12.	$[Cu_2(BDPT^{4-})(H_2O)_2]$	HNUST-1	1400	156.4	31.2	39.8	7.2	25
13.	$[Zn(hfipbb)(bpt)]_n{\cdot}n(DMF)_2{\cdot}n(H_2O)$ (1)		77*	21.4	33.6	-	-	26
14.	UiO-66(Hf)-$(COOH)_2$		378	37.4	28.2	-	-	27
	UiO-66(Hf)-$(F)_4$		329	27.55	23.4	-	-	
15.	Al(Sbpdc)(OH)	USTC-253	1800	82.4	25.5	-	-	28
16.	UiO-66(Zr)-$(OCH_2CH_3)_2$		405	23.07	26.2	-	-	29
	UiO-66(Zr)-$(F)_4$		833	47.26	18.7	-	-	
	UiO-66(Zr)-$(COOH)_4$		212	18.03	30.5	-	-	
17.	$[Cu_2PDAI(H_2O)]$	PCN-124	1372	204	26.3	-	20	30
18.	$\{[Zn_2(TPOM)(3,7\text{-}DBTDC)_2]$ $\cdot 7H_2O \cdot DMA\}_n$		267**	28.2	34.1	124.8	3	31
	$\{[Cd_2(TPOM)(3,7\text{-}DBTDC)_2]$ $\cdot 6H_2O \cdot 3DMF\}$		432**	37.8	31.7	47.6	12.3	
19.	$[Zn(btz)]{\cdot}DMF{\cdot}0.5H_2O\}_n$ (H_2btz = 1,5-bis(5-tetrazolo)-3-oxapentane	Zn-btz	1151	181.24	31.2	-	21.1	32
20.	$Al_4(OH)_2(OCH_3)_4(BDC\text{-}NH_2)_3$	CAU-1	1268	161.28	~48	101	-	33
21.		NU-1000	2320	31	17	-	-	34
22.	$[\{Zn(BINDI)_{0.5}(bpa)_{0.5}(H_2O)\}.4H_2O]_n$	MOF1	84*	22.8	33.8	-	-	35
23.	$\{[Zn(SDB)(3,3'\text{-}L)_{0.5}]{\cdot}xG\}_n$	IITKGP-13A	206**	45.02	25	76	9.8	36
	$\{[Zn_2(SDB)_2(4,4'\text{-}L)]{\cdot}xG\}_n$	IITKGP-13B	129**	18.59	20.83	-	-	
24.	$Zn(5\text{-}mtz)_2{\cdot}$guest (5-Hmtz 5-methyltetrazole)	TTF-4	1172	67.6	16.7	-	-	37
25.	$\{[Cu_2(4\text{-}TPOM)(3,7\text{-}DBTDC)_2]{\cdot}4H_2O{\cdot}3DMF\}_n$ (1)	-	385**	63	24	1942	34	38
26.		LIFM-33	1588	80.4	39.7	33	-	39
27.	$\{[Zn_5(dmtrz)_3(IPA)_3(OH)]{\cdot}DMF{\cdot}H_2O\}_n$	MAC-4	796	33.6	21	-	-	40
	$\{[Zn_5(dmtrz)_3(OH\text{-}IPA)_3(OH)]{\cdot}DMF{\cdot}5H_2O\}n$	MAC-4-OH	339	69.44	31	-	-	

28.	$Mg_2(dondc)(en)_{1.5}(H_2O)_{0.5}$		1553	58.24	44	116	-	[41]
29.	$\{[Co(BDC)(L)\cdot 2H_2O]\cdot xG\}_n$	CoMOF-2	6.8	~51	35	-	-	[42]
30.	$Cu_2(BPnDC)_2(bpy)$	SNU-6	2590	50.4	-	-	-	[43]
31.		Ni-MOF-1	152	37.57	36.57	42.89	-	[44]
32.	$[Cd(\boldsymbol{L1})_2]\cdot 2DMF$	7a	18	28.29	24.02	157.6	6.1	[45]
	$[Cd(\boldsymbol{L2})_2]\cdot 2DMF$	8a	23	53.65	34.92	322.2	10.0	
33.	$[Cu_{1.5}(\boldsymbol{L})(bpy)]\cdot DMF\cdot 1.5H_2O$	CSMCRI-13	79	75.17	28.57	-	-	[46]
34.	rht-MOF-1		2100	112.4	28.5	-	36	[47]
35.	$\{[Zn(CHDC)(L)].H_2O\}_n$ (1)	--	7	4		-	-	[48]
	$\{[Cd(CHDC)(L)].H_2O\}_n$ (2)		19	6		-	-	
36.	$[Cu(BDC\text{-}NO_2)(DMF)]\cdot x$Solvents	CuBDC-NO_2-a	523	73.92	20.2	-	-	[49]
37.	$\{[Zn(SDB)(L)_{0.5}]\cdot S\}_n$	IITKGP-5	366	-	56.4	435.5	151.6	[50]
38.	$([NH_2(CH_3)_2][Cu_2O(Ad)(BDC)]\cdot(H_2O)_2($DMA)	IISERP-MOF26	210.6	22	96.32	160	15	[51]
39.	$Co_2(ad)_2(CO_2CH_3)_2\cdot 2DMF\cdot 0.5H_2O$	bio-MOF-11	1040	45	134.4	81	-	[52]
40.	$\{[Zn_3(DMF)(btrm)(bdc)_3]\cdot nDMF\}_\infty$	MOF1	20	17.9	-	21.1	-	[53]
			92**					
41.	$[Zn_2(L)(bpb)_2](NO_3)(DMF)_3(H_2O)$	-	425	19.9	54.3	181	-	[54]
42.	$\{[Zn(H_2L_1)(L_2)]\cdot DMF\cdot 2H_2O\}_n$	-	-	52.1	21.3	22	11	[55]
43.	$Zr_6O_4(OH)_4(BDC)_6$	UiO-66(Zr)	1390	49.28	26.3	37.5	-	[56]
44.	$Cu_3(BTC)_2$	HKUST-1	1400	156.3	31.2		-	[57]
45.		UiO-66-NH_2	1258	70.56@298K	-	-	32.3	[58]
46.		PCN-88	3308	160	27		18	[59]
47.	$Cr_3O(H_2O)_2F(BDC)_3$	MIL-101(Cr)	2166	22.6	-	20.2	-	[60]
48.	$[Cu_2(BDPT^{4-})(H_2O)_2]$	HNUST-1	1400	156	31.2	39.8	7.2	[25]
49.	$[Cd_3(TCA)_2\boldsymbol{L}(H_2O)_2]\cdot 2DMA\cdot 11H_2O$	Activated Framework	503	53.06	32.2	237	8	**This work**

*CO_2@273 K **CO_2@195 K ***Langmuir

Table S5. A comparison of catalytic performance of activated framework to that of other MOF materials in CO_2 cycloaddition.

S.No.	MOF	Reaction Conditions	Model Substrate	Conversion/ Yield (%)	Ref.
1.	Mg-MOF-74	100 °C, 19.7 bar, 4 h	Styrene oxide	95	[61]
2.	NH_2–MIL–101(Al)	120 °C, 18 bar, 6h	Styrene oxide	96	[62]
3.	$[Zn_2(PZDC)(1/2ATZ)_2(H_2O)_2\cdot 2.5H_2O]$	90 °C, 10 bar, 6 h	Propylene oxide	94	[63]
4	$[\{Co(4,4'\text{- bipy})(L\text{-cys})(H_2O)\cdot H_2O\}_n$ (2 D- CCB)	120℃, 1 bar, 56 h	Styrene oxide	85	[64]
5.	$[Cu_5(TPTC)_3(BPDC\text{-Urea})_{0.5}(H_2O)_5]$ (1-Urea)	RT, 30 h, 1 atm	Propylene oxide	98	[65]
6.	$\{[Zn_2(TBIB)_2(HTCPB)_2]\cdot 9DMF\cdot 19H_2O\}_n$	RT, 24 h , 1 atm	Styrene oxide	>99	[66]
7.	$[\{Sm(BTB)(H_2O)\}\cdot H_2O]n$	80 °C, 1 bar, 15 h	Styrene oxide	93	[67]
	$[\{Gd(BTB)(H_2O)\}\cdot H_2O]n$		Styrene oxide	93	
8.	$[Zn_3(BTC)_2]$	130 °C, 13 bar, 6 h	Styrene oxide	99.05	[68]
9.	Ni-TCPE1	100 ℃, 10 bar,12 h	Styrene oxide	100	[69]
	Ni-TCPE2			86.2	
10.	$[Zn_3(BTC)_2]$	130 °C, 13 bar, 6 h	Styrene oxide	>99	[68]
11.	Mg-MOF	60 ℃, 1 bar, 24 h	Epichlorohydrin	99	[70]
12.	ZIF-8	80 °C, 6.9 bar, 5 h	Styrene oxide	39.4	[71]
13.	Co-MOF-74	100 °C, 2 MPa, 4 h	Styrene oxide	96	[72]
14.	Ni@ZrOF	70 °C, 1 MPa; 6 h	Styrene Oxide	97.6	[73]
15.	CSMCRI-13	70 °C, 8 bar, 6 h	Propylene Oxide	>99	[46]

16.	Cu-NTTA	100 °C, 10 bar, 8 h	Glycidyl Phenyl Ether	95.9	[74]
17.	DUT-52(Zr)	80 °C, 1.2 MPa, 6 h	Epichlorohydrin	>99	[75]
18.	CSMCRI-9	65 °C, 10 bar, 6 h	Styrene oxide	99.9	[76]
19.	ADES-3	80 °C, 10 bar, 8 h	Styrene oxide	99	[77]
20.	Hf-NU-1000	RT, 1 bar, 56 h	Styrene oxide	100	[78]
21.	UiO–67–IL	90 °C, 1 bar, 12 h	Epichlorohydrin	98	[79]
22.	MOF-892	80 °C, 1 bar, 16h	Styrene oxide	82	[80]
23.	InDCPN-Cl	80 °C, 1 bar, 24 h	Styrene oxide	71	[81]
24.	NUC-5	80 °C, 1 bar, 24 h	Styrene oxide	99	[82]
25.	UMCM-1-NH_2	RT, 12 bar, 24 h	Propylene Oxide	53	[83]
26.	$[Cd_3(TCA)_2\boldsymbol{L}(H_2O)_2]\cdot 2DMA\cdot 11H_2O$	50 °C, 0.5 MPa, 4h	Styrene oxide	99.9	**This Work**

References

1. G. Sheldrick, SHELXS, University of Göttingen, Germany (1997);(c) W. Madison, Bruker APEX2 Software, Bruker AXS Inc. V2. 0-1, USA (2005);(d) GM Sheldrick, *J SADABS, Program for Empirical Absorption Correction of Area Detector Data*, 1997.
2. G. Sheldrick, SAINT and XPREP, version 5.1, *J Siemens Industrial Automation Inc., Madison, WI*, 1995.
3. S. Bruker, Bruker AXS Inc., Madison, Wisconsin, USA, Version 6.02 (includes XPREP and SADABS), 1999.
4. O. V. Dolomanov, L. J. Bourhis, R. J. Gildea, J. A. K. Howard and H. Puschmann, OLEX2: A Complete Structure Solution, Refinement and Analysis Program, *J. Appl. Crystallogr.*, 2009, **42**, 339.
5. G. Sheldrick, SHELXL-2014/7, University of Gottingen, Germany, 2014 Search PubMed;(b) L. Farrugia, *J. Appl. Crystallogr*, 2012, **45**, 849-854.
6. G. M. Sheldrick, Crystal Structure Refinement with SHELXL. Acta Crystallographica, *Acta Crystallogr., Sect. C: Struct. Chem.*, 2015, **71**, 3.
7. G. M. Sheldrick, Crystal Structure Refinement with SHELXL, *Acta Crystallogr., Sect. C: Struct. Chem.*, 2015, **71**, 3.
8. A. Spek, Single-Crystal Structure Validation with the Program Platon, *J. Appl. Crystallogr.*, 2003, **36**, 7-13.
9. V. A. Blatov, A. P. Shevchenko and D. M. Proserpio, Applied Topological Analysis of Crystal Structures with the Program Package TOPOSPRO, *Cryst. Growth Des.*, 2014, **14**, 3576-3586.
10. N. Seal, R. Goswami, M. Singh, R. S. Pillai and S. Neogi, An Ultralight Charged MOF as Fluoro-Switchable Monitor for Assorted Organo-Toxins: Size-Exclusive Dye Scrubbing and Anticounterfeiting Applications *via* Tb^{3+} Sensitization, *Inorg. Chem. Front.*, 2021, **8**, 296-310.
11. M. Singh and S. Neogi, Urea-Engineering Mediated Hydrogen-Bond Donating Friedel–Crafts Alkylation of Indoles and Nitroalkenes in a Dual-Functionalized Microporous Metal–Organic Framework with High Recyclability and Pore-Fitting-Induced Size-Selectivity, *Inorg. Chem. Front.*, 2022, **9**, 1897-1911.
12. J. Taesch, V. Heitz, F. Topić and K. Rissanen, Templated synthesis of a large and flexible covalent porphyrinic cage bearing orthogonal recognition sites, *Chem. Commun.*, 2012, **48**, 5118-5120.
13. M. Horeau, G. Lautrette, B. Wicher, V. Blot, J. Lebreton, M. Pipelier, D. Dubreuil, Y. Ferrand and I. Huc, Metal-Coordination-Assisted Folding and Guest Binding in Helical

Aromatic Oligoamide Molecular Capsules, *Angew. Chem. Int. Ed.*, 2017, **56**, 6823-6827.
14. L. Pan, K. M. Adams, H. E. Hernandez, X. Wang, C. Zheng, Y. Hattori and K. Kaneko, Porous Lanthanide-Organic Frameworks: Synthesis, Characterization, and Unprecedented Gas Adsorption Properties, *J. Am. Chem. Soc.*, 2003, **125**, 3062-3067.
15. Y.-W. Li, J.-R. Li, L.-F. Wang, B.-Y. Zhou, Q. Chen and X.-H. Bu, Microporous Metal–Organic Frameworks with Open Metal Sites as Aorbents for Selective Gas Adsorption and Fluorescence Sensors for Metal Ions, *J. Mater. Chem. A*, 2013, **1**, 495-499.
16. P. Tshuma, B. C. E. Makhubela, C. A. Ndamyabera, S. A. Bourne and G. Mehlana, Synthesis and Characterization of 2D Metal-Organic Frameworks for Adsorption of Carbon Dioxide and Hydrogen, *Front. Chem.*, 2020, **8**, 581226.
17. C. Chen, M. Zhang, W. Zhang and J. Bai, Stable Amide-Functionalized Metal–Organic Framework with Highly Selective CO_2 Adsorption, *Inorg. Chem.*, 2019, **58**, 2729-2735.
18. Y. E. Cheon and M. P. Suh, Selective Gas Adsorption in a Microporous Metal–organic Framework Constructed of Co^{II4} Clusters, *Chem. Commun.*, 2009, DOI: 10.1039/B900085B, 2296-2298.
19. T. Wu, J. Zhang, C. Zhou, L. Wang, X. Bu and P. Feng, Zeolite RHO-Type Net with the Lightest Elements, *J. Am. Chem. Soc.*, 2009, **131**, 6111-6113.
20. P.-Q. Liao, D.-D. Zhou, A.-X. Zhu, L. Jiang, R.-B. Lin, J.-P. Zhang and X.-M. Chen, Strong and Dynamic CO_2 Sorption in a Flexible Porous Framework Possessing Guest Chelating Claws, *J. Am. Chem. Soc.*, 2012, **134**, 17380-17383.
21. W. J. Phang, H. Jo, W. R. Lee, J. H. Song, K. Yoo, B. Kim and C. S. Hong, Superprotonic Conductivity of a UiO-66 Framework Functionalized with Sulfonic Acid Groups by Facile Postsynthetic Oxidation, *Angew. Chem. Int. Ed.*, 2015, **54**, 5142-5146.
22. G. Zhang, G. Wei, Z. Liu, S. R. J. Oliver and H. Fei, A Robust Sulfonate-Based Metal–Organic Framework with Permanent Porosity for Efficient CO_2 Capture and Conversion, *Chem. Mater.*, 2016, **28**, 6276-6281.
23. M. Singh and S. Neogi, Selective and Multicyclic CO_2 Adsorption with Visible Light-Driven Photodegradation of Organic Dyes in a Robust Metal–Organic Framework Embracing Heteroatom-Affixed Pores, *Inorg. Chem.*, 2022, **61**, 10731-10742.
24. M.-H. Yu, P. Zhang, R. Feng, Z.-Q. Yao, Y.-C. Yu, T.-L. Hu and X.-H. Bu, Construction of a Multi-Cage-Based MOF with a Unique Network for Efficient CO_2 Capture, *ACS Appl. Mater. Interfaces*, 2017, **9**, 26177-26183.
25. B. Zheng, H. Liu, Z. Wang, X. Yu, P. Yi and J. Bai, Porous NbO-type metal–organic framework with inserted acylamide groups exhibiting highly selective CO_2 capture, *CrystEngComm*, 2013, **15**, 3517-3520.
26. N. Chatterjee and C. L. Oliver, A Dynamic, Breathing, Water-Stable, Partially Fluorinated, Two-Periodic, Mixed-Ligand Zn(II) Metal–Organic Framework Modulated by Solvent Exchange Showing a Large Change in Cavity Size: Gas and Vapor Sorption Studies, *Cryst. Growth Des.*, 2018, **18**, 7570-7578.
27. Z. Hu, A. Nalaparaju, Y. Peng, J. Jiang and D. Zhao, Modulated Hydrothermal Synthesis of UiO-66(Hf)-Type Metal–Organic Frameworks for Optimal Carbon Dioxide Separation, *Inorg. Chem.*, 2016, **55**, 1134-1141.
28. Z.-R. Jiang, H. Wang, Y. Hu, J. Lu and H.-L. Jiang, Polar Group and Defect Engineering in a Metal–Organic Framework: Synergistic Promotion of Carbon Dioxide Sorption and Conversion, *ChemSusChem*, 2015, **8**, 878-885.

29. Z. Hu, Y. Peng, Z. Kang, Y. Qian and D. Zhao, A Modulated Hydrothermal (MHT) Approach for the Facile Synthesis of UiO-66-Type MOFs, *Inorg. Chem.*, 2015, **54**, 4862-4868.
30. J. Park, J.-R. Li, Y.-P. Chen, J. Yu, A. A. Yakovenko, Z. U. Wang, L.-B. Sun, P. B. Balbuena and H.-C. Zhou, A Versatile Metal–Organic Framework for Carbon Dioxide Capture and Cooperative Catalysis, *Chem. Commun.*, 2012, **48**, 9995-9997.
31. G. Chakraborty, P. Das and S. K. Mandal, Polar Sulfone-Functionalized Oxygen-Rich Metal–Organic Frameworks for Highly Selective CO_2 Capture and Sensitive Detection of Acetylacetone at ppb Level, *ACS Appl. Mater. Interfaces*, 2020, **12**, 11724-11736.
32. P. Cui, Y.-G. Ma, H.-H. Li, B. Zhao, J.-R. Li, P. Cheng, P. B. Balbuena and H.-C. Zhou, Multipoint Interactions Enhanced CO_2 Uptake: A Zeolite-like Zinc–Tetrazole Framework with 24-Nuclear Zinc Cages, *J. Am. Chem. Soc.*, 2012, **134**, 18892-18895.
33. X. Si, C. Jiao, F. Li, J. Zhang, S. Wang, S. Liu, Z. Li, L. Sun, F. Xu, Z. Gabelica and C. Schick, High and Selective CO_2 Uptake, H_2 Storage and Methanol Sensing on the Amine-decorated 12-connected MOF CAU-1, *Energy Environ. Sci.*, 2011, **4**, 4522-4527.
34. P. Deria, J. E. Mondloch, E. Tylianakis, P. Ghosh, W. Bury, R. Q. Snurr, J. T. Hupp and O. K. Farha, Perfluoroalkane Functionalization of NU-1000 via Solvent-Assisted Ligand Incorporation: Synthesis and CO_2 Adsorption Studies, *J. Am Chem. Soc.*, 2013, **135**, 16801-16804.
35. S. S. Dhankhar, N. Sharma and C. M. Nagaraja, Construction of Bifunctional 2-fold Interpenetrated Zn(II) MOFs Exhibiting Selective CO_2 Adsorption and Aqueous-phase Sensing of 2,4,6-Trinitrophenol, *Inorg. Chem. Front.*, 2019, **6**, 1058-1067.
36. S. Chand, A. Pal, R. Saha, P. Das, R. Sahoo, P. K. Chattaraj and M. C. Das, Two Closely Related Zn(II)-MOFs for their Large Difference in CO_2 Uptake Capacities and Selective CO_2 Sorption, *Inorg. Chem.*, 2020, **59**, 7056-7066.
37. Y.-H. Tang, F. Wang, J.-X. Liu and J. Zhang, Diverse Tetrahedral Tetrazolate Frameworks with N-rich Surface, *Chem. Commun.*, 2016, **52**, 5625-5628.
38. G. Chakraborty, P. Das and S. K. Mandal, Efficient and Highly Selective CO_2 Capture, Separation, and Chemical Conversion under Ambient Conditions by a Polar-Group-Appended Copper(II) Metal–Organic Framework, *Inorg. Chem.*, 2021, **60**, 5071-5080.
39. C.-X. Chen, Z. Wei, J.-J. Jiang, Y.-Z. Fan, S.-P. Zheng, C.-C. Cao, Y.-H. Li, D. Fenske and C.-Y. Su, Precise Modulation of the Breathing Behavior and Pore Surface in Zr-MOFs by Reversible Post-Synthetic Variable-Spacer Installation to Fine-Tune the Expansion Magnitude and Sorption Properties, *Angew. Chem. Int. Ed.*, 2016, **55**, 9932-9936.
40. Y. Ling, F. Yang, M. Deng, Z. Chen, X. Liu, L. Weng and Y. Zhou, Novel Iso-Reticular Zn(II) Metal–Organic Frameworks constructed by Trinuclear-Triangular and Paddle-Wheel Units: Synthesis, Structure and Gas Adsorption, *Dalton Trans.*, 2012, **41**, 4007-4011.
41. J. S. Yeon, W. R. Lee, N. W. Kim, H. Jo, H. Lee, J. H. Song, K. S. Lim, D. W. Kang, J. G. Seo, D. Moon, B. Wiers and C. S. Hong, Homodiamine-functionalized metal-organic frameworks with a MOF-74-type extended structure for superior selectivity of CO2 over N-2, *Journal of Materials Chemistry A*, 2015, **3**, 19177-19185.
42. B. Parmar, P. Patel, R. S. Pillai, R. K. Tak, R. I. Kureshy, N.-u. H. Khan and E. Suresh, Cycloaddition of CO_2 with an Epoxide-Bearing Oxindole Scaffold by a Metal–Organic Framework-Based Heterogeneous Catalyst under Ambient Conditions, *Inorg. Chem.*, 2019, **58**, 10084-10096.

43. H. J. Park and M. P. Suh, Mixed-Ligand Metal–Organic Frameworks with Large Pores: Gas Sorption Properties and Single-Crystal-to-Single-Crystal Transformation on Guest Exchange, *Chem. Eur J.*, 2008, **14**, 8812-8821.
44. L. Wang, R. Zou, W. Guo, S. Gao, W. Meng, J. Yang, X. Chen and R. Zou, A New Microporous Metal-Organic Framework with a Novel Trinuclear Nickel Cluster for Selective CO_2 Adsorption, *Inorg. Chem. Commun.*, 2019, **104**, 78-82.
45. M. Singh, A. S. Palakkal, R. S. Pillai and S. Neogi, N-Functionality Actuated Improved CO_2 Adsorption and Turn-On Detection of Organo-Toxins with Guest-Induced Fluorescence Modulation in Isostructural Diamondoid MOFs, *J. Mater. Chem. C*, 2021, **9**, 7142-7153.
46. N. Seal and S. Neogi, Intrinsic-Unsaturation-Enriched Biporous and Chemorobust Cu(II) Framework for Efficient Catalytic CO_2 Fixation and Pore-Fitting Actuated Size-Exclusive Hantzsch Condensation with Mechanistic Validation, *ACS Appl. Mater. Interfaces*, 2021, **13**, 55123-55135.
47. W.-Y. Gao, T. Pham, K. A. Forrest, B. Space, L. Wojtas, Y.-S. Chen and S. Ma, The Local Electric Field Favours more than Exposed Nitrogen Atoms on CO_2 Capture: A Case Study on the rht-type MOF Platform, *Chem. Commun.*, 2015, **51**, 9636-9639.
48. B. Parmar, P. Patel, R. I. Kureshy, N.-u. H. Khan and E. Suresh, Sustainable Heterogeneous Catalysts for CO_2 Utilization by Using Dual Ligand ZnII/CdII Metal–Organic Frameworks, *Chem. Eur. J.*, 2018, **24**, 15831-15839.
49. H. Cui, Y. Ye, T. Liu, Z. A. Alothman, O. Alduhaish, R.-B. Lin and B. Chen, Isoreticular Microporous Metal–Organic Frameworks for Carbon Dioxide Capture, *Inorg. Chem.*, 2020, **59**, 17143-17148.
50. A. Pal, S. Chand, S. M. Elahi and M. C. Das, A microporous MOF with a polar pore surface exhibiting excellent selective adsorption of CO_2 from CO_2–N_2 and CO_2–CH_4 gas mixtures with high CO_2 loading, *Dalton Trans.*, 2017, **46**, 15280-15286.
51. R. Maity, H. D. Singh, A. K. Yadav, D. Chakraborty and R. Vaidhyanathan, Water-stable adenine-based MOFs with polar pores for selective CO_2 capture, *Chem. Asian J.*, 2019, **14**, 3736-3741.
52. J. An, S. J. Geib and N. L. Rosi, High and selective CO_2 uptake in a cobalt adeninate metal−organic framework exhibiting pyrimidine- and amino-decorated pores, *J. Am. Chem. Soc.*, 2010, **132**, 38-39.
53. T. S. Sukhikh, E. Y. Filatov, A. A. Ryadun, K. A. Kovalenko and A. S. Potapov, Structural diversity and carbon dioxide sorption selectivity of Zinc(II) metal-organic frameworks based on Bis(1,2,4-triazol-1-yl)methane and terephthalic acid, *Molecules*, 2022, **27**, 6481.
54. S. Sen, S. Neogi, A. Aijaz, Q. Xu and P. K. Bharadwaj, Construction of non-interpenetrated charged metal–organic frameworks with doubly pillared layers: Pore modification and selective gas adsorption, *Inorg. Chem.*, 2014, **53**, 7591-7598.
55. S. Sen, S. Neogi, A. Aijaz, Q. Xu and P. K. Bharadwaj, Structural variation in Zn(II) coordination polymers built with a semi-rigid tetracarboxylate and different pyridine linkers: synthesis and selective CO_2 adsorption studies, *Dalton Trans.*, 2014, **43**, 6100-6107.
56. C. Hon Lau, R. Babarao and M. R. Hill, A Route to Drastic Increase of CO_2 Uptake in Zr Metal Organic Framework UiO-66, *Chem. Commun.*, 2013, **49**, 3634-3636.
57. C. Chen, B. Li, L. Zhou, Z. Xia, N. Feng, J. Ding, L. Wang, H. Wan and G. Guan, Synthesis of Hierarchically Structured Hybrid Materials by Controlled Self-Assembly of Metal–Organic Framework with Mesoporous Silica for CO_2 Adsorption, *ACS Appl. Mater. Interfaces*, 2017, **9**, 23060-23071.

58. H. Molavi, A. Eskandari, A. Shojaei and S. A. Mousavi, Enhancing CO_2/N_2 adsorption selectivity via post-synthetic modification of NH_2-UiO-66(Zr), *Microporous Mesoporous Mater.*, 2018, **257**, 193-201.
59. J.-R. Li, J. Yu, W. Lu, L.-B. Sun, J. Sculley, P. B. Balbuena and H.-C. Zhou, Porous Materials with Pre-Designed Single-Molecule Traps for CO_2 Selective Adsorption, *Nat. Commun.*, 2013, **4**, 1538.
60. C. Chen, N. Feng, Q. Guo, Z. Li, X. Li, J. Ding, L. Wang, H. Wan and G. Guan, Template-directed fabrication of MIL-101(Cr)/mesoporous silica composite: Layer-packed structure and enhanced performance for CO_2 capture, *J. Colloid Interface Sci.*, 2018, **513**, 891-902.
61. D.-A. Yang, H.-Y. Cho, J. Kim, S.-T. Yang and W.-S. Ahn, CO_2 capture and conversion using Mg-MOF-74 prepared by a sonochemical method, *Energy Environ. Sci.*, 2012, **5**, 6465-6473.
62. S. Senthilkumar, M. S. Maru, R. S. Somani, H. C. Bajaj and S. Neogi, Unprecedented NH_2-MIL-101(Al)/n-Bu_4NBr System as Solvent-Free Heterogeneous Catalyst for Efficient Synthesis of Cyclic Carbonates via CO_2 cycloaddition, *Dalton Trans.*, 2018, **47**, 418-428.
63. Y. Li, X. Zhang, P. Xu, Z. Jiang and J. Sun, The Design of a Novel and Resistant Zn(PZDC)(ATZ) MOF Catalyst for the Chemical Fixation of CO_2 under Solvent-Free Conditions, *Inorg. Chem. Front.*, 2019, **6**, 317-325.
64. A. C. Kathalikkattil, R. Roshan, J. Tharun, H.-G. Soek, H.-S. Ryu and D.-W. Park, Pillared Cobalt–Amino Acid Framework Catalysis for Styrene Carbonate Synthesis from CO_2 and Epoxide by Metal–Sulfonate–Halide Synergism, *ChemCatChem*, 2014, **6**, 284-292.
65. L.-Q. Wei and B.-H. Ye, Efficient conversion of CO_2 via grafting urea group into a $[Cu_2(COO)_4]$-based metal–organic framework with hierarchical porosity, *Inorg. Chem.*, 2019, **58**, 4385-4393.
66. R. A. Agarwal, A. K. Gupta and D. De, Flexible Zn-MOF Exhibiting Selective CO_2 Adsorption and Efficient Lewis Acidic Catalytic Activity, *Cryst. Growth Des.*, 2019, **19**, 2010-2018.
67. B. Ugale, S. S. Dhankhar and C. M. Nagaraja, Exceptionally Stable and 20-Connected Lanthanide Metal–Organic Frameworks for Selective CO_2 Capture and Conversion at Atmospheric Pressure, *Cryst. Growth Des*, 2018, **18**, 2432-2440.
68. C. Feng, X. Cao, L. Zhang, C. Guo, N. Akram and J. Wang, Zn 1,3,5-Benzenetricarboxylate as an Efficient Catalyst for the Synthesis of Cyclic Carbonates from CO_2, *RSC Adv.*, 2018, **8**, 9192-9201.
69. Z. Zhou, C. He, J. Xiu, L. Yang and C. Duan, Metal–Organic Polymers Containing Discrete Single-Walled Nanotube as a Heterogeneous Catalyst for the Cycloaddition of Carbon Dioxide to Epoxides, *J. Am. Chem. Soc.*, 2015, **137**, 15066-15069.
70. R. Das, T. Ezhil, A. S. Palakkal, D. Muthukumar, R. S. Pillai and C. M. Nagaraja, Efficient Chemical Fixation of CO_2 from Direct Air under Environment-Friendly Co-catalyst and Solvent-free Ambient Conditions, *J. Mater. Chem. A*, 2021, **9**, 23127-23139.
71. M. Zhu, D. Srinivas, S. Bhogeswararao, P. Ratnasamy and M. A. Carreon, Catalytic Activity of ZIF-8 in the Synthesis of Styrene Carbonate from CO_2 and Styrene Oxide, *Catal. Commun.*, 2013, **32**, 36-40.
72. H.-Y. Cho, D.-A. Yang, J. Kim, S.-Y. Jeong and W.-S. Ahn, CO_2 Adsorption and Catalytic Application of Co-MOF-74 Synthesized by Microwave Heating, *Catal. Today*, 2012, **185**, 35-40.

73. M. Singh, P. Solanki, P. Patel, A. Mondal and S. Neogi, Highly Active Ultrasmall Ni Nanoparticle Embedded inside a Robust Metal–Organic Framework: Remarkably Improved Adsorption, Selectivity, and Solvent-Free Efficient Fixation of CO_2, *Inorg. Chem.*, 2019, **58**, 8100-8110.
74. X. Guo, Z. Zhou, C. Chen, J. Bai, C. He and C. Duan, New rht-type metal–organic frameworks decorated with acylamide groups for efficient carbon dioxide capture and chemical fixation from raw power plant flue gas, *ACS Appl. Mater. Interfaces*, 2016, **8**, 31746-31756.
75. J. F. Kurisingal, Y. Rachuri, A. S. Palakkal, R. S. Pillai, Y. Gu, Y. Choe and D.-W. Park, Water-Tolerant DUT-Series Metal–Organic Frameworks: A Theoretical–Experimental Study for the Chemical Fixation of CO_2 and Catalytic Transfer Hydrogenation of Ethyl Levulinate to γ-Valerolactone, *ACS Appl. Mater. Interfaces*, 2019, **11**, 41458-41471.
76. N. Seal, M. Singh, S. Das, R. Goswami, B. Pathak and S. Neogi, Dual-Functionalization Actuated Trimodal Attribute in an Ultra-Robust MOF: Exceptionally Selective Capture and Effectual Fixation of CO_2 with Fast-responsive, Nanomolar Detection of Assorted Organo-Contaminants in Water, *Mater. Chem. Front.*, 2021, **5**, 979-994.
77. U. Patel, P. Patel, B. Parmar, A. Dadhania and E. Suresh, Synergy of Dual Functional Sites for Conversion of CO_2 in a Cycloaddition Reaction under Solvent-Free Conditions by a Zn(II)-Based Coordination Network with a Ladder Motif, *Cryst. Growth Des.*, 2021, **21**, 1833-1842.
78. H. Beyzavi, R. C. Klet, S. Tussupbayev, J. Borycz, N. A. Vermeulen, C. J. Cramer, J. F. Stoddart, J. T. Hupp and O. K. Farha, A Hafnium-Based Metal–Organic Framework as an Efficient and Multifunctional Catalyst for Facile CO_2 Fixation and Regioselective and Enantioretentive Epoxide Activation, *J. Am. Chem. Soc.*, 2014, **136**, 15861-15864.
79. L.-G. Ding, B.-J. Yao, W.-L. Jiang, J.-T. Li, Q.-J. Fu, Y.-A. Li, Z.-H. Liu, J.-P. Ma and Y.-B. Dong, Bifunctional Imidazolium-Based Ionic Liquid Decorated UiO-67 Type MOF for Selective CO_2 Adsorption and Catalytic Property for CO_2 Cycloaddition with Epoxides, *Inorg. Chem.*, 2017, **56**, 2337-2344.
80. P. T. K. Nguyen, H. T. D. Nguyen, H. N. Nguyen, C. A. Trickett, Q. T. Ton, E. Gutiérrez-Puebla, M. A. Monge, K. E. Cordova and F. Gándara, New Metal–Organic Frameworks for Chemical Fixation of CO_2, *ACS Appl. Mater. Interfaces*, 2018, **10**, 733-744.
81. Y. Yuan, J. Li, X. Sun, G. Li, Y. Liu, G. Verma and S. Ma, Indium–Organic Frameworks Based on Dual Secondary Building Units Featuring Halogen-Decorated Channels for Highly Effective CO_2 Fixation, *Chem. Mater.*, 2019, **31**, 1084-1091.
82. H. Chen, L. Fan, X. Zhang and L. Ma, Nanocage-Based $In^{III}\{Tb^{III}\}_2$-Organic Framework Featuring Lotus-Shaped Channels for Highly Efficient CO_2 Fixation and I_2 Capture, *ACS Appl. Mater. Interfaces*, 2020, **12**, 27803-27811.
83. R. Babu, A. C. Kathalikkattil, R. Roshan, J. Tharun, D.-W. Kim and D.-W. Park, Dual-porous metal organic framework for room temperature CO_2 fixation via cyclic carbonate synthesis, *Green Chem.*, 2016, **18**, 232-242.